FFIBM/766/130

Approved
Kjeller 11 September 2003

Bjarne Haugstad
Director of Research

EVERYTHING YOU WANTED TO KNOW ABOUT MATERIAL TESTING BUT WERE AFRAID TO ASK

TELAND Jan Arild, SVINSÅS Eirik

FFI/RAPPORT–2003/00155

FORSVARETS FORSKNINGSINSTITUTT
Norwegian Defence Research Establishment
Postboks 25, 2027 Kjeller, Norge

FORSVARETS FORSKNINGSINSTITUTT (FFI)
Norwegian Defence Research Establishment
P O BOX 25
NO–2027 KJELLER, NORWAY

UNCLASSIFIED

SECURITY CLASSIFICATION OF THIS PAGE
(when data entered)

REPORT DOCUMENTATION PAGE

1) PUBL/REPORT NUMBER	2) SECURITY CLASSIFICATION	3) NUMBER OF PAGES
FFI/RAPPORT–2003/00155	UNCLASSIFIED	51
1a) PROJECT REFERENCE	**2a) DECLASSIFICATION/DOWNGRADING SCHEDULE**	
FFIBM/766/130		

4) TITLE

EVERYTHING YOU WANTED TO KNOW ABOUT MATERIAL TESTING BUT WERE AFRAID TO ASK

(ALT DU ØNSKET Å VITE OM MATERIALTESTING, MEN VAR REDD FOR Å SPØRRE OM)

5) NAMES OF AUTHOR(S) IN FULL (surname first)

TELAND Jan Arild, SVINSÅS Eirik

6) DISTRIBUTION STATEMENT

Approved for public release. Distribution unlimited
(Offentlig tilgjengelig)

7) INDEXING TERMS

IN ENGLISH:	IN NORWEGIAN:
a) Material testing	a) Materialtesting
b) GREAC cell	b) GREAC celle
c) Split Hopkinson Bar	c) Split Hopkinson Bar
d) Flyer Plate	d) Flyer Plate
e) Concrete	e) Betong

THESAURUS REFERENCE:

8) ABSTRACT

The theory behind various methods of material testing is reviewed. We look in detail at static triaxial testing with a GREAC cell and dynamic testing with the Split Hopkinson Bar and Flyer plate. In particular, we discuss the testing of concrete using these methods.

9) DATE	AUTHORIZED BY This page only	POSITION
11 September 2003	Bjarne Haugstad	Director of Research

ISBN-82-464-0838-0

UNCLASSIFIED

SECURITY CLASSIFICATION OF THIS PAGE
(when data entered)

CONTENTS

EVERYTHING YOU WANTED TO KNOW ABOUT MATERIAL TESTING BUT WERE AFRAID TO ASK

1 INTRODUCTION

To give accurate predictions about dynamic processes involving specific materials, it is necessary to know how the relevant materials behave under various circumstances. A way of finding this out, is by performing material tests, in which the material is subjected to different types of loading. On the basis of the test results, a mathematical model describing the material can be constructed. Unfortunately, real materials turn out to behave in a very complicated fashion, strongly dependent on how the external forces are applied. As a consequence, it is very difficult to create a complete material model that is valid for every type of loading. Instead, one aims at constructing a model that reflects the behaviour of the material under loadings that are relevant for the particular process under study.

Several different methods for testing a material have been developed over the years. In this report we take a close look at the most important ones, describing the theory behind them and their strengths and weaknesses.

The tests can roughly be divided into two groups, namely static and dynamic tests. As the name indicates, in static tests the load on the material is applied very slowly, while in dynamic tests the material is loaded very quickly.

The following tests are covered in the report:

- GREAC cell
- Split Hopkinson Bar
- Flyer Plate

In the report we first emphasize the mathematical description of the “ideal tests”, i.e. we momentarily ignore practical problems that will arise when the tests are performed. Having completed this, we try to examine the practical problems, whether they are important, how they can be avoided and ways to live with them.

2 PRELIMINARY THEORY FOR STATIC TESTING

We will start by describing static concrete testing in detail. However, before developing the mathematical theory, it will be useful to examine material behaviour under states of uniaxial stress and uniaxial strain.

In Teland (1) mathematical expressions for these cases of loading were given in cartesian coordinates for a rectangular specimen. Here we present the expressions in cylindrical coordinates for a cylindrical specimen. They are seen to be very similar.

2.1 Uniaxial stress

Ideally the specimen is under uniaxial stress during a standard compressive test. The elastic stress and strain behaviour of the material is given by:

$$\sigma_r = \sigma_\theta = 0 \quad , \quad \sigma_z = E\epsilon_z \tag{2.1}$$

$$\epsilon_r = \epsilon_\theta = -\nu\epsilon_z \tag{2.2}$$

Consequently we have:

$$\sigma_{vm} = \sqrt{3J_2} = |\sigma_z| \quad , \quad p = \frac{\sigma_z}{3} \tag{2.3}$$

where J_2 is the second stress invariant. When the yield limit is reached, the material turns plastic. During plasticity, the following condition must be satisfied:

$$\sigma_{vm} = Y(p) \tag{2.4}$$

Since $\sigma_r = \sigma_\theta$ also during plasticity, Equation (2.3) still holds and on inserting into Equation (2.4) is seen to produce only one equation for one unknown quantity, σ_z. The equation then has a unique solution, and can only be satisfied for one value of σ_z and thus one value of p. Consequently we can not detemine the yield stress as a function of pressure with this test, since it becomes impossible to increase the pressure further once yielding has been achieved (although the strain can be increased indefinitely). A uniaxial stress test therefore only provides us with with one single point on the yield curve.

2.2 Uniaxial strain

If the material is unable to expand laterally while being compressed axially, it is said to be in a state of uniaxial strain. The elastic behaviour is then as follows:

$$\sigma_r = \sigma_\theta = \left(\frac{E\nu}{(1+\nu)(1-2\nu)}\right)\epsilon_z \quad , \quad \sigma_z = \left(\frac{E(1-\nu)}{(1+\nu)(1-2\nu)}\right)\epsilon_z \tag{2.5}$$

$$\epsilon_r = \epsilon_\theta = 0 \tag{2.6}$$

We then have:

$$\sigma_{vm} = \sqrt{3J_2} = |\sigma_z - \sigma_r| = \left(\frac{E}{1+\nu}\right)\epsilon_z = 2G\epsilon_z \tag{2.7}$$

$$p = \frac{2\sigma_r + \sigma_z}{3} = \frac{E}{3(1-2\nu)}\epsilon_z = K\epsilon_z \tag{2.8}$$

Combining Equations (2.7) and (2.8) gives us:

$$\sigma_{vm} = 3\left(\frac{1-2\nu}{1+\nu}\right)p \tag{2.9}$$

During plasticity, the following conditions must be satisfied:

$$\sigma_{vm} = |\sigma_z - \sigma_r| = Y(p) \tag{2.10}$$

$$p = \frac{2\sigma_r + \sigma_z}{3} \tag{2.11}$$

Since σ_r is not identically zero in this case, we see that Equation (2.10) is one equation with two unknowns. Thus, neither σ_r nor σ_z are fixed, which means that the pressure can be varied during plastic flow. A uniaxial strain test can therefore be used to determine part of the yield curve *Y(p)*. This is done by recording the relationship between σ_{vm} and p during plastic flow.

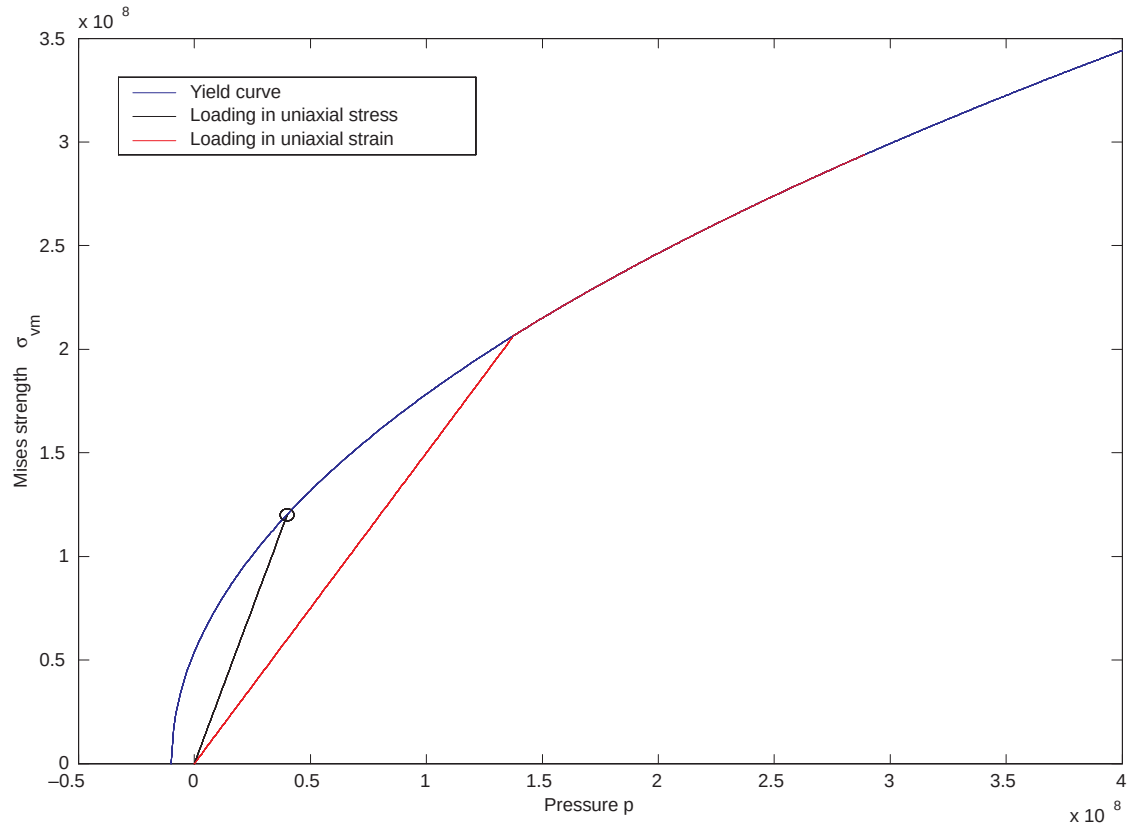

Figure 3.2: Loading paths in stress space for uniaxial stress and strain tests. Unlike the uniaxial strain test, the uniaxial stress test does not move along the yield curve and can therefore only be used for determining a single point on this curve.

In Figure 3.2 we have illustrated the situation for loading under uniaxial stress and strain. We notice that on using the uniaxial strain loading, we miss out on information about the yield curve for low pressures. Performing a uniaxial stress test in addition, enables us to find one additional point lower on the yield curve.

Similarly, by combining the pressure and density we can obtain the equation of state (EOS). In this ideal case, the EOS is easily seen to be linear, but for real materials like concrete it will be more complicated.

2.3 More complicated loading

An interesting question is now the following: Does the yield curve only depend on the pressure (as indicated in the above chapters) or is it a function of other parameters as well?

The answer is that it depends on which material we are studying. For some materials (metals) the yield curve is even independent of pressure and is, in effect, a yield limit, while for other materials it depends on the pressure only. Further, for materials such as concrete things are even more complicated.

For concrete, a stress state where $\sigma_z > \sigma_r = \sigma_\theta$ will not give the same yield stress as a state where $\sigma_z < \sigma_r = \sigma_\theta$ even when the value of $\sqrt{J_2}$ is identical. Thus, for concrete, yielding is defined by a yield surface in some kind of stress space instead of a yield curve or yield limit. We will briefly see this in Chapter 4.5 where we examine the output from a so–called GREAC cell test. For more details, the reader should consult Riedel (4) and references therein.

3 STANDARD STATIC CONCRETE TESTS

The previous chapter dealt only with theory, whereas in this chapter we briefly look at the practical application of the theory to standard uniaxial concrete testing.

In the most common material test, only the compressive strength σ_c of the concrete is measured. The test is very simple: One takes a concrete cube (or cylinder) of a specified size and increases the axial stress until the concrete breaks. The corresponding stress is called the compressive strength. Similarly there are standard tensile tests for determining the concrete tensile strength.

All these “engineering tests” have in common that they have not been designed to determine material properties for input into hydrocodes for advanced numerical simulations. Rather they are meant to be standard methods for classification of concrete. Further description of such methods is given in (5) and (6).

Obviously a compression test is relevant for the strength of a bridge beam, but in every construction there will be induced complicated tri–axial stress states. However, compressive strength could still be used as a relevant parameter in empirical calculations since there is an (unknown) relation between uniaxial and triaxial properties.

In this report, our focus will be on tri–axial tests to determine hydrocode data (or similar) and not on the standard “engineering” tests.

4 GREAC CELL TEST

In this chapter we will discuss the GREAC (Gauged REActive Confinement) cell test method. It is a static triaxial method in which a test specimen is confined inside a cylinder and then loaded axially. A schematic view of the GREAC cell is shown in Figure 3.1. Such an apparatus has been built and used in material testing at FFI.

By measuring the strains on the outside of the cylinder, we shall see that a great deal of information about the material properties of the specimen can be extracted. Of special interest is the yield limit as a function of pressure *Y(p)* and the equation of state $p(\rho)$.

Unlike in the uniaxial strain case, the steel confinement is not infinitely strong which means that there will be strains in the cylinder. This is actually a good thing because by measuring these strains, we are able to deduce the stress state in the concrete specimen.

To distinguish the quantities in the steel cylinder and the concrete specimen without having indices all over the place, we are going to denote concrete quantities with a "hat", $\hat{\sigma}_{ij}$, and steel cylinder quantities without.

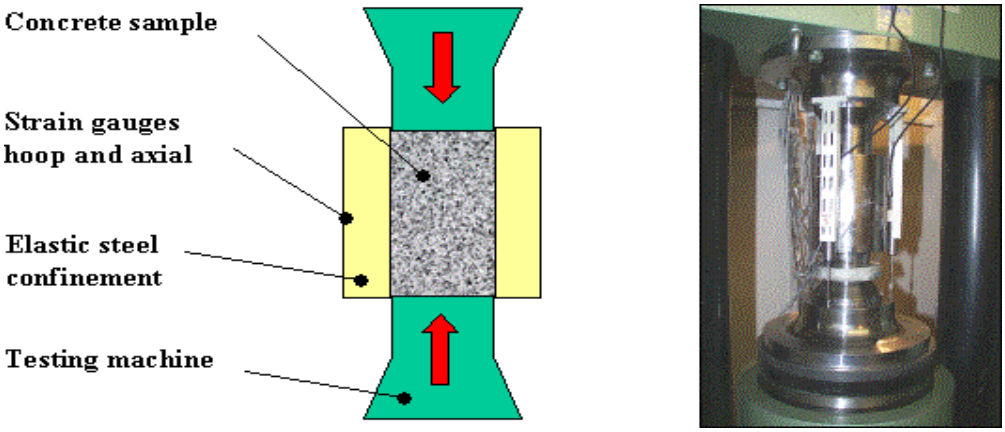

Figure 4.1: GREAC cell

4.1 Experimentally measured quantities

By placing strain gauges on the steel cylinder and by recording the force on the piston, we can perform measurements that eventually enables us to calculate various physical quantities. Although it can be a huge challenge to relate measurements of electrical voltages with strains in the cylinder, we will ignore this problem here, and just assume that the following quantities are measured directly:

- Axial force on the concrete $\hat{F}$
- Axial displacement of the concrete $\hat{u}_z$
- Axial strain on the outside boundary of the confining cylinder $\epsilon_z(b)$
- Angular strain on the outside boundary of the steel cylinder $\epsilon_\theta(b)$

This is all well and good, but as we have seen, expressions for the pressure $\hat{p}$, the density $\hat{\rho}$ and von Mises stress $\hat{\sigma}_{vm}$ in the concrete specimen are what is really needed. Since we are unable to measure any of these directly, it is necessary to figure out a way of calculating them in terms of the quantities given above. To accomplish this, we need to examine the GREAC cell test mathematically.

4.2 Mathematical description of the test

Since $\hat{\sigma}_r = \hat{\sigma}_\theta$ in the specimen (and consequently $\hat{\epsilon}_r = \hat{\epsilon}_\theta$), it becomes slightly easier to calculate $\hat{p}$, $\hat{\rho}$ and $\hat{\sigma}_{vm}$. Using this and assuming all non–diagonal components of the stress tensor to vanish, we have the same relations as for uniaxial strain:

$$\hat{p} = \frac{1}{3}\left(2\hat{\sigma}_r + \hat{\sigma}_z\right) \tag{4.1}$$

$$\hat{\sigma}_{vm} = |\hat{\sigma}_r - \hat{\sigma}_z| \tag{4.2}$$

Note that an alternative to the von Mises stress is to use the Tresca stress $\hat{\sigma}_T$, given by:

$$\hat{\sigma}_T = \max\left(|\hat{\sigma}_r - \hat{\sigma}_\theta|, |\hat{\sigma}_r - \hat{\sigma}_z|, |\hat{\sigma}_\theta - \hat{\sigma}_z|\right) \tag{4.3}$$

In our GREAC cell case, the von Mises stress is easily seen to be identical to the Tresca stress.

The density $\hat{\rho}$ can be calculated from the strains using the following relation:

$$\hat{\rho} = \frac{\hat{\rho}_0}{J} = \frac{\hat{\rho}_0}{1 + \hat{\epsilon}_V} \tag{4.4}$$

where $\hat{\epsilon}_V$ is called the volumetric strain. It is given in terms of the principal strains by a very complicated expression (see Equation (2.43) in Teland (1)), but in the absence of shear strains and using that $\hat{\epsilon}_r = \hat{\epsilon}_\theta$, it may be written as:

$$\hat{\epsilon}_V = (1 + \hat{\epsilon}_r)^2(1 + \hat{\epsilon}_z) - 1 \simeq 2\hat{\epsilon}_r + \hat{\epsilon}_z \tag{4.5}$$

Now, say we start loading the concrete specimen at the time $t = 0$, and keep loading it for a while. It is now clear that by recording data for the quantities $\hat{\epsilon}_r$, $\hat{\epsilon}_z$, $\hat{\sigma}_r$, $\hat{\sigma}_z$ in the concrete as a function of time, the corresponding density, pressure and Mises stress as functions of time can easily be calculated. This then enables us to determine the pressure as a function of density, which is the equation of state, and Mises stress as function of pressure, which during plasticity is equal to the yield curve.

The only remaining problem is how to calculate the stresses and strains mentioned above. As we saw earlier, none of them are measured directly in the test.

However, at least the axial strain $\hat{\epsilon}_z$ can be easily calculated:

Axial strain in the concrete: $$\hat{\epsilon}_z = \frac{\hat{u}_z}{L}$$

where L is the (initial) length of the concrete specimen. Since $\hat{u}_z$ is independent of r, so is obviously the axial strain $\hat{\epsilon}_z$.

So, that's one down, three to go. Unfortunately, calculating the remaining three variables as a function of the measured variables is not equally simple. One method is to use the FFI Matlab Toolbox (2) designed for this purpose. This toolbox has the option of finding numerical solutions by using a Finite Element Method. However, it is also possible to find (very good) approximate analytical expressions, as will be described below.

4.2.1 Boundary conditions and assumptions

The concrete specimen is assumed to be loaded so slowly that the sistuation can be treated as static.

Due to the angular symmetry of the GREAC cell, all angular derivatives vanish and there is no displacement in the θ–direction. Further, we assume that the axial strain is independent of radial position. In the steel cylinder we therefore have:

$$u_r = u(r) \quad , \quad u_\theta = 0 \quad , \quad u_z = \epsilon_z^0 z \tag{4.6}$$

On considering the complete GREAC cell, we realise that the radial stress $\hat{\sigma}_r$ in the specimen (which we know is equal to the angular stress $\hat{\sigma}_\theta$) will be equal to the stress at the material boundary since the radial stress must be continuous across the boundary. Thus:

$$\hat{\sigma}_r = \hat{\sigma}_\theta = \sigma_r^a \tag{4.7}$$

This will be used to simplify our mathematical model of the GREAC cell somewhat. Instead of examining the complete set–up we will only look at the confining steel cylinder with inner radius a and outer radius b. Due to the specimen expanding, the cylinder is loaded radially at the inner surface by a given stress σ_r^a. Instead of calculating σ_r^a from the applied axial load on the concrete, we take $\sigma_r(a) = \sigma_r^a$ as a boundary condition, where of course σ_r^a is so far unknown. Our goal will therefore be to express it in terms of the measured quantities $\epsilon_\theta(b)$ and $\epsilon_z(b)$.

Another boundary condition is zero radial stress at the outer surface, $\sigma_r(b) = 0$. Further, a natural boundary condition would be $\sigma_{zz} = 0$ in the steel cylinder. This means a stress free boundary and corresponds to a specific strain ϵ_{zz}. However, it turns out that the mathematics is not much more complicated if we assume something a little more general, namely a specific constant strain ϵ_z^0. Physically this means that a certain axial stress is applied to the cylinder in order to achieve a specific strain ϵ_z^0. The special case of $\sigma_{zz} = 0$ can then later be obtained as a special case.

4.2.2 Analytical solution

In cylindrical coordinates, the radial equilibrium equation takes the following form:

$$\frac{\partial \sigma_r}{\partial r} + \frac{\sigma_r - \sigma_\theta}{r} = 0 \tag{4.8}$$

which on using Hooke's law and the symmetry considerations of Equation (4.6) gives the following equation for the strains:

$$\frac{\partial^2 u}{\partial r^2} + \frac{1}{r}\frac{\partial u}{\partial r} - \frac{u}{r^2} = 0 \tag{4.9}$$

This equation has the following solution:

$$u(r) = Ar + \frac{B}{r} \tag{4.10}$$

The constants A and B are determined according to the boundary conditions $\sigma_r(a) = \sigma_r^a$ and $\sigma_r(b) = 0$. This gives us:

$$A = -\frac{(1+\nu)(1-2\nu)}{E\left(\left(\frac{b}{a}\right)^2 - 1\right)}\sigma_r^a - \nu\epsilon_z \tag{4.11}$$

$$B = -\frac{\sigma_r^a}{2G}\left[\frac{b^2}{\left(\frac{b}{a}\right)^2 - 1}\right] \tag{4.12}$$

where E and ν are the elastic constants of the steel cylinder (not the concrete). For the stresses and strains, we thus have:

$$\sigma_r(r) = \sigma_r^a\left[\frac{\left(\frac{b}{r}\right)^2 - 1}{\left(\frac{b}{a}\right)^2 - 1}\right] \tag{4.13}$$

$$\sigma_\theta(r) = \sigma_r^a\left[\frac{\left(\frac{b}{r}\right)^2 + 1}{\left(\frac{b}{a}\right)^2 - 1}\right] \tag{4.14}$$

$$\epsilon_r(r) = \frac{\sigma_r^a(1+\nu)}{E\left(\left(\frac{b}{a}\right)^2 - 1\right)}\left(\left(\frac{b}{r}\right)^2 - 1 + 2\nu\right) \tag{4.15}$$

$$\epsilon_\theta(r) = \frac{\sigma_r^a(1+\nu)}{E\left(\left(\frac{b}{a}\right)^2 - 1\right)}\left(-\left(\frac{b}{r}\right)^2 - 1 + 2\nu\right) \tag{4.16}$$

Using these equations, we eventually are able to express the radial stress at the inner boundary as a function of measured quantities at the outer boundary:

$$\sigma_r^a = \hat{\sigma}_r = -\frac{1}{2}\left(\left(\frac{b}{a}\right)^2 - 1\right)\sigma_\theta(b) = -\frac{1}{2}\left(\left(\frac{b}{a}\right)^2 - 1\right)\frac{E}{1-\nu^2}\left(\epsilon_\theta(b) + \nu\epsilon_z\right) \tag{4.17}$$

The radial stress must be continuous across the boundary, so σ_r^a is also the radial stress in the concrete (assumed the same everywhere).

The radial strain at the boundary is given by:

$$\epsilon_r(a) = \hat{\epsilon}_r = -\nu\epsilon_z - \frac{\left(\left(\frac{b}{a}\right)^2 - 1 + 2\nu\right)}{2(1-\nu)}\left(\epsilon_\theta(b) + \nu\epsilon_z\right) \tag{4.18}$$

Finally, we can calculate the axial stress $\hat{\sigma}_z$:

$$\hat{\sigma}_z = -\frac{F}{\pi a^2(1+\hat{\epsilon}_r)^2}, \tag{4.19}$$

The expressions derived above are correct if the cylinder is sufficiently long to avoid edge effects near the top and bottom. However, the strain gauges are placed in the middle and should not be much affected by such effects.

Another assumption is that friction is negligible. If there is friction between the specimen and the cylinder, there will be shear stresses in the material and our calculated stress distribution will not be correct.

A way of approximately taking these shear stresses into account is as follows. Let us assume that the expression for axial stress is modified in the following way:

$$\hat{\sigma}_z = -\frac{F+S}{\pi a^2(1+\hat{\epsilon}_r)^2}, \tag{4.20}$$

where *S* is the total shear force on the concrete specimen.

The shear force is balanced by axial stresses in the cylinder. If we assume the axial stress to be independent of *r*, the shear stress becomes:

$$S = a^2\pi\left((\frac{b}{a})^2 - 1\right)\sigma_z^b, \tag{4.21}$$

The shear stress is given through σ_z^b which is not a measured quantity. However, using Hooke's law, it can be expressed as a function of the measured quantities:

$$\sigma_z^b = \frac{E}{1-\nu^2}(\epsilon_z^b + \nu\epsilon_\theta^b). \tag{4.22}$$

In an ideal situation we of course have $\sigma_z = 0$ (even as a boundary condition), in which case *S = 0*. In fact, putting $\sigma_z = 0$ we find that our expressions simplify to:

$$\sigma_r^a = -\frac{1}{2}\left(\left(\frac{b}{a}\right)^2 - 1\right)E\epsilon_\theta(b) \tag{4.23}$$

$$\epsilon_r^a = \frac{1}{2}\left((1-\nu) - (1+\nu)\left(\frac{b}{a}\right)^2\right)\epsilon_\theta(b) \tag{4.24}$$

$$\epsilon_z^b = -\nu\epsilon_\theta(b) \tag{4.25}$$

These expressions above relied on the assumption that the axial stress was constant inside the cylinder, which is generally not correct. However, it is possible to account for this numerically, as is done in the FFI Matlab GREAC cell toolbox using a finite element model. Using this code, it can however be shown that there is little difference in results between the finite element and thick cylinder theory calculations, provided that the strain is measured in the middle of the cylinder.

4.3 Elastic constants

In addition, the GREAC cell can also be used to obtain estimates for the elastic constants of the concrete. To do this, we have to assume that the stress state is close to uniaxial strain.

The shear modulus G is then found according to Equation (2.7) by measuring the slope of $\hat{\sigma}_{vm}$ as a function of $\hat{\epsilon}_z$ during an elastic loading and unloading cycle.

The Bulk modulus K is found according to Equation (2.8) by measuring the slope of $\hat{p}$ as a function of $\hat{\epsilon}_z$ during an elastic loading and unloading cycle.

However, it must be noted that this method may not be well–defined, since in practise it may be difficult to distinguish the elastic and plastic part of the loading/unloading process, even for an almost ideal material. Alternative methods, for example involving measurements of density and sound velocity, are likely to be more accurate for determining elastic properties.

4.4 Double GREAC cell

In a test with the GREAC cell, the maximum axial force that can be applied is determined by either the power of the testing machine, the yield strength of the confining cylinder or the yield strength of the pistons. Naturally, a tougher material may be used for the critical components, but as far as the cylinder is concerned, an even more clever approach can be learned from gun tube manufacturing.

If the cylinder is constructed from two layers, it is possible to pre–stress the inner part by machining the outer sleeve slightly too small, heat it so that it expands until it can be fitted and then do the final assembly. As the outer sleve cools, a radial stress will be induced in the inner part. When the device is to be used in a test later, the expanding pressure from the specimen first has to overcome the negative elastic pre–stress in the confining material. In principle, the acceptable load may be doubled by this approach. The two parts of the cylinder can be of the same material, but often the combined effect of both crimping and a strong material in the inner part will be useful. The outer part, which does experience less radial stress, will usually be of steel or similar.

FFI has designed and built such a “double GREAC cell”, using an inner cylinder of tungsten and the outer cylinder of steel. Since tungsten has a higher yield limit than steel, such a GREAC cell is able to withstand larger stresses before yielding occurs and it thereby becomes possible to obtain concrete data at higher pressures than with a single steel GREAC cell.

Let us now look briefly at the mathematical problem for a double GREAC cell. In principle this is relatively easy to define. Denoting the inner boundary by a, the material interface by b and the outer boundary by c, the boundary conditions are now given by:

$$\sigma_r(a) = \sigma_r^a \quad , \quad \sigma_r(c) = 0 \tag{4.26}$$

$$\sigma_r^1(b) = \sigma_r^2(b) \quad , \quad u^1(b) = u^2(b) \tag{4.27}$$

In a real situation, the axial strain will be a function of radius. The inner cylinder will shrink in the axial direction and friction with the outer cylinder will tend to drag this one along. However, we ignore this small effect and instead, for simplicity, assume that the two cylinders stick together so that the (constant) axial strain is equal in both of them:

$$\epsilon_z^1(b) = \epsilon_z^2(b) \tag{4.28}$$

This assumption implies that the corresponding axial stresses $\sigma_z^1(b)$ and $\sigma_z^2(b)$ must be different since the cylinders have different elastic properties. Actually the axial stress σ_z will be a function of radius instead of being constant on the two cylinders. However, as a first approximation we try two different types of boundary condition, namely $\sigma_z^1 = 0$ or $\sigma_z^2 = 0$, respectively.

Using either of these conditions, the problem is completely defined. However, although the boundary conditions are simple, the mathematical expressions unfortunately become much more complicated than for the single GREAC cell. In fact, the final expressions take up at least one page, so we will not reproduce them here. Instead it is more convenient to use a Matlab routine that has been developed for these calculations.

On using the Matlab routine with realistic data for the FFI double GREAC cell, it was seen that for $\sigma_z^1 = 0$, we obtain $\sigma_z^2 = 0.17\sigma_r(b)$. In the case of $\sigma_z^2 = 0$, we find a value of $\sigma_z^1 = 0.29\sigma_r(b)$. The “true” value will probably lie somewhere in between. On considering the friction between two metals, it is seen that the ratios calculated above are reasonable, so that the cylinders will stick together and the assumption of continous axial strain is okay.

The concrete properties can now be calculated in a similar way as for a regular (single) GREAC cell.

4.5 GREAC cell data example

In this section we present data from a real GREAC cell test performed at FFI. In Figure 4.2 we have plotted results for the stress difference $\sigma_z - \sigma_r$ as a function of pressure *p*.

Because of symmetry, the stress difference is equal to the Mises stress. We note that the concrete approaches a yield limit of approximately 250 MPa for higher pressures. There are some oscillations especially early in the process due to noise from the experimental set–up and the combination of signals.

It is interesting to examine the unloading part of the curve. By plotting the Mises stress (absolute value of the stress difference), we notice that the Mises stress does not quite reach as high as during loading. A possible interpretation could be that the yield limit has been reduced as a result of damage, but this is not the case since during re–loading, we reach the “old” yield limit again.

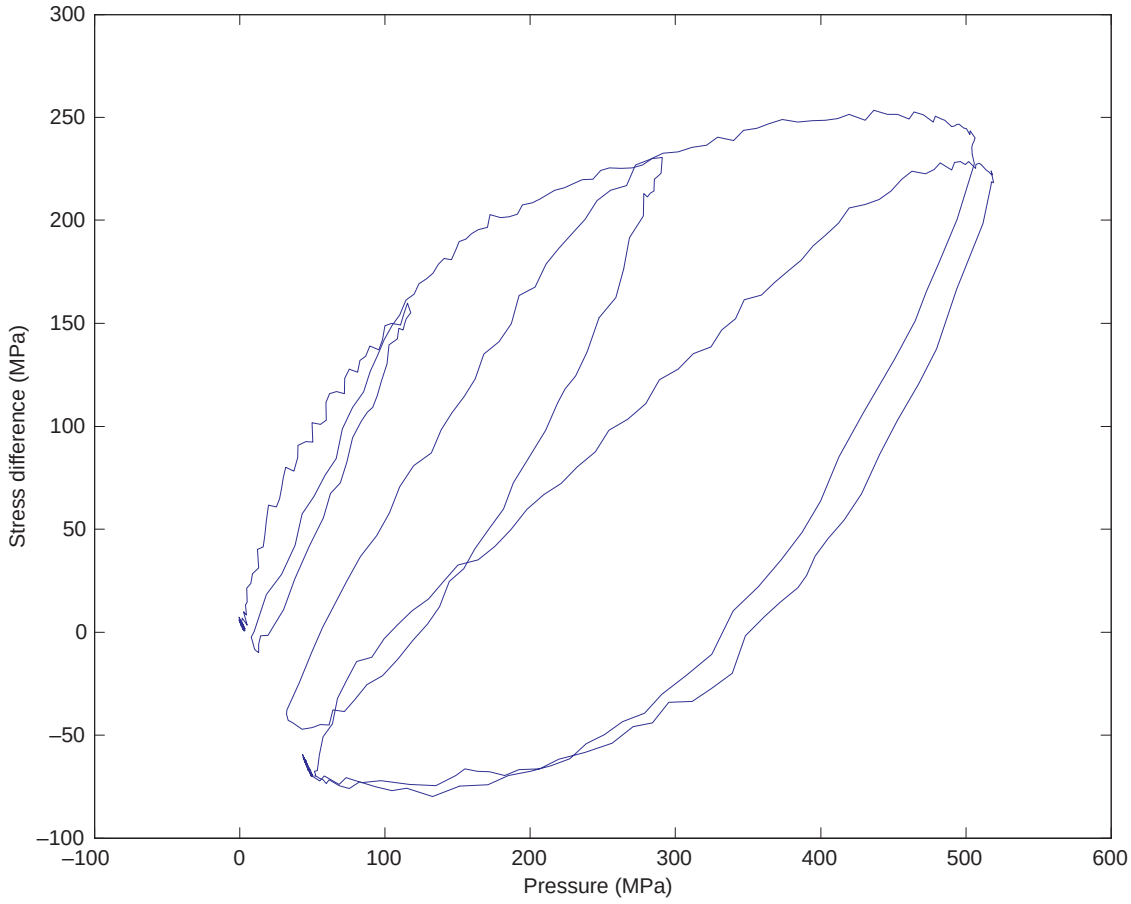

Figure 4.2: GREAC cell stress difference data from a real test.

Instead, this indicates what we mentioned in Chapter 2.3, namely that the concrete is described by a complicated yield surface which is a function of more variables than just pressure. During compression the loading is said to be on the "compressive meridian" since $\sigma_z > \sigma_r = \sigma_\theta$, whereas during (the final part of) unloading we have $\sigma_z < \sigma_r = \sigma_\theta$ which is called the "tensile meridian". Thus, a GREAC cell test gives us information about the yield limit under both these types of loading.

In the pressure range for this specific case, we further note that the loading–unloading loops show more and more hysteresis with time. This is due to dissipation of energy as a results of increased damage during loading.

5 HOEK CELL

Unfortunately, there is a problem with the GREAC cell approach that we have not mentioned yet. So far we have been concerned with determining the yield stress *Y* as a function of pressure, *Y(p)*. However, for concrete the yield stress turns out to depend on another variable called damage *D* as well, i.e. *Y=Y(p,D)*. Damage is usually defined as a variable that lies in the range between 0 and 1, where *D=0* means that no damage has been inflicted on the material, whereas *D=1* means that it has been completely destroyed.

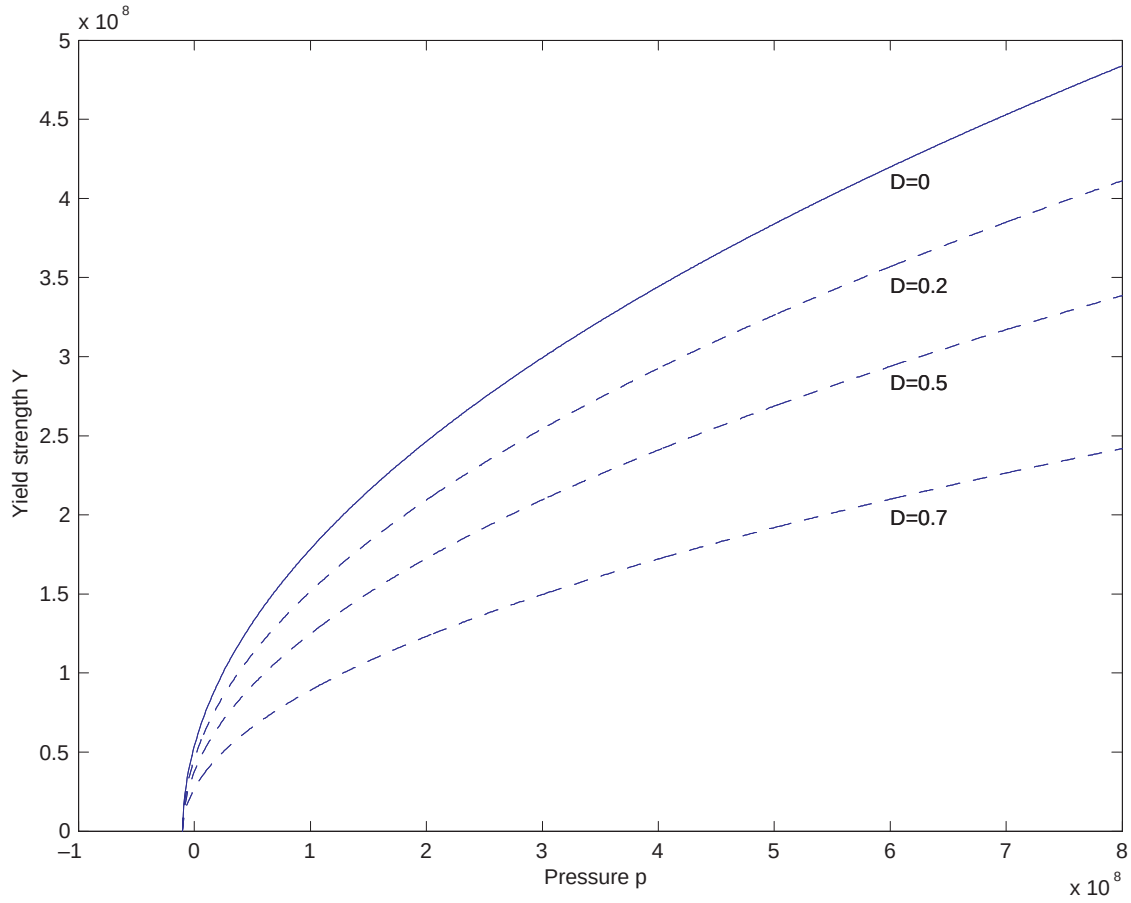

Figure 4.3: Possible yield curves for various values of the damage parameter.

What is this damage thing? It depends on the material in question. During loading of concrete, which we are particularly interested in, internal microcraking will degrade the load–carrying capacity. However, we will not be concerned with the actual physical mechanisms on a microscopic level in this report. Instead we will assume that, although the exact relationship is unknown, the yield stress will decrease in some way as the damage parameter increases. This is illustrated in Figure 4.3, where we have plotted how the yield strength could depend on the pressure for various values of the damage parameter.

In the mathematical description, damage is usually assumed to be an increasing function of the accumulated plastic strain in the concrete. Thus, for constant plastic strain, the damage should be constant. This is where the problem with the GREAC cell occurs. As the load increases, the plastic strain is not constant, and consequently the damage D is not constant either. In fact, the damage is increasing, and we appear to be recording the yield stress for a concrete that becomes more and more damaged. This means that during a GREAC cell test we are not obtaining a yield curve at constant damage, but actually a curve for a steadily increasing (but unknown) value of the damage parameter. This is illustrated in Figure 4.4.

Does this mean that all the GREAC cell results are invalid and the GREAC cell test pointless? Not necessarily, because the HOEK cell comes to the rescue!

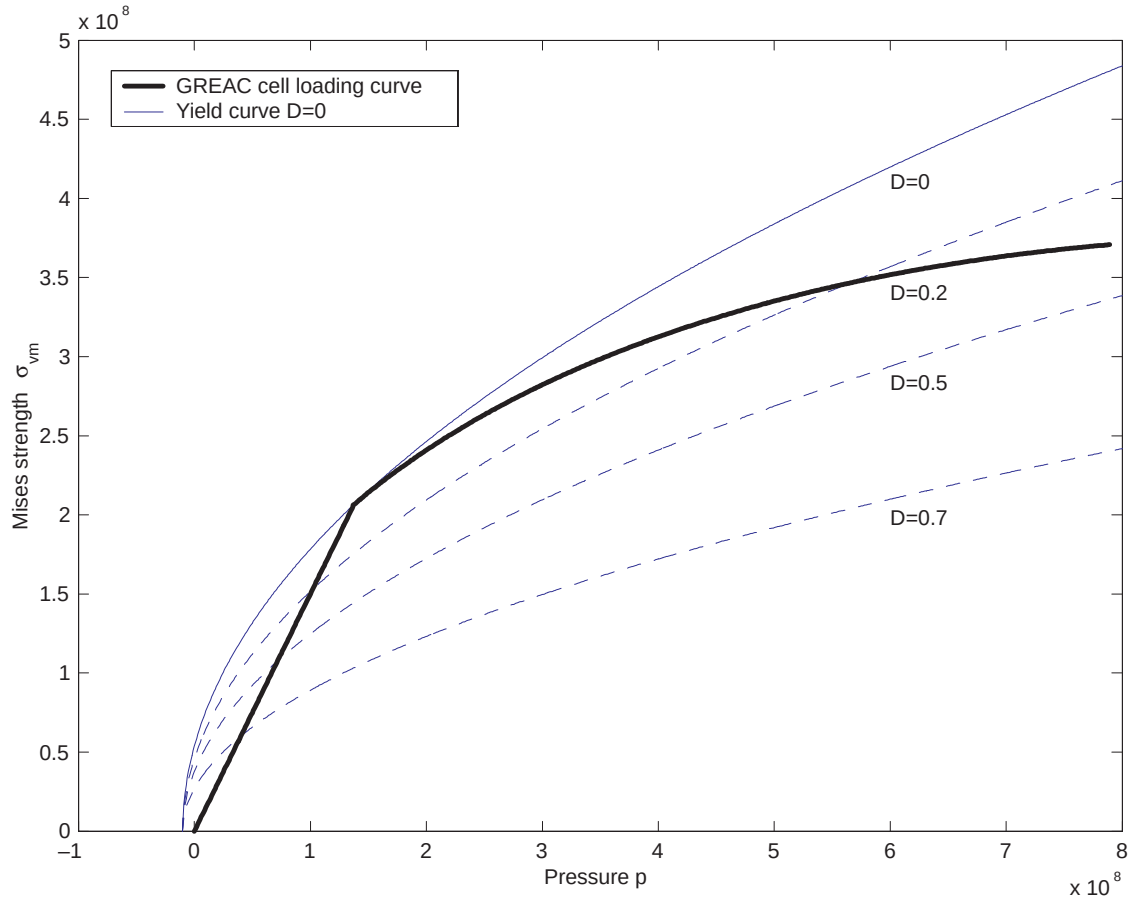

Figure 4.4: During a GREAC cell test the damage may not be constant and thus the yield curve obtained is not for constant D=0. (This is a theoretical plot not based on any experimental data).

A HOEK cell can be described as a more advanced version of the GREAC cell, where the confining pressure can be controlled independently of the axial pressure. In the HOEK cell, the test specimen is instead surrounded by a rubber sleeve and a hydraulic liquid whose pressure can be adjusted. The rubber sleeve may be stabilized by metal ribs or similar devices.

The ability of a HOEK cell setup to control the pressure independently makes it possible to investigate different stress paths during testing, for instance a pure hydrostatic compression followed by shear. This can be exploited to eliminate the problem described for the GREAC cell. Instead of moving along the yield curve and increasing the damage while testing, we may instead follow a different path in stress space by first increasing the pressure and then the shear stress. In this way we reach the *D=0* yield curve at a different pressure.

There is a major drawback with the HOEK cell, though. When the concrete specimen fails globally, the oil / rubber confinement does not offer sufficient support to prevent a (partial) collapse. For this reason, only one data point for the maximum failure, or shear strength can be generated with each test sample, unlike the GREAC cell where we (before we realised that damage was not constant) could generate a large part of the yield curve.

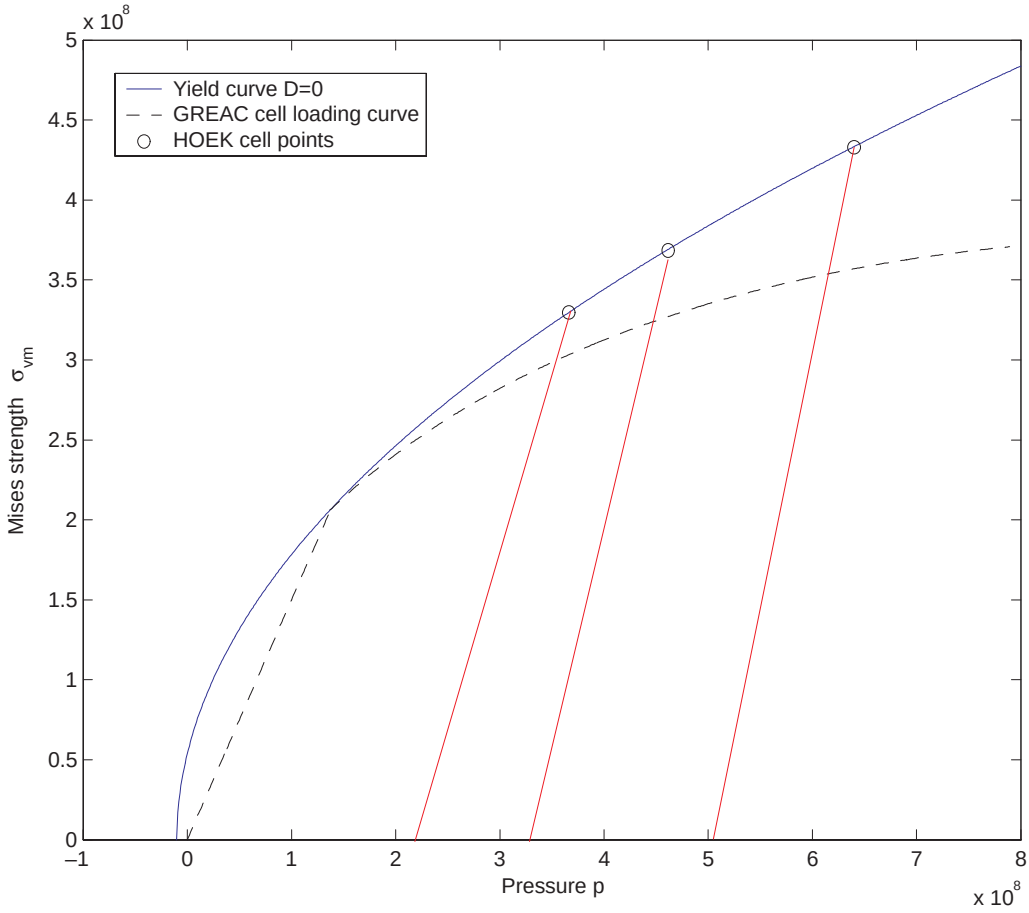

Figure 4.5: By performing various Hoek Cell tests we can obtain different points on the D=0 yield curve.

To obtain more data points, it is therefore necessary to test more concrete samples. This process is illustrated in Figure 4.5.

It is inconvenient to obtain all of the *D=0* yield curve from a HOEK cell test, as doing this requires a lot of testing on different concrete samples. However, a possible short–cut is to first perform a GREAC cell test to find most of the yield curve (for unknown values of the damage parameter), and then afterwards performing a HOEK cell test to find one point (preferably for large pressure) on the *D=0* yield curve. If we then normalise the curve obtained from the GREAC cell so that it fits with the one point obtained from the HOEK cell, the result for the other normalised points might possible not be far away from the actual yield curve.

Note that even pure hydrostatic compression will induce some internal microcracking and hence some damage, so the method is not perfect. However, in all real loading situations where the yield limit is reached, the material will undergo a phase of “pre–damage”. The HOEK–cell minimizes this and therefore represents the optimal situation of achievable material strength.

This concludes our review of static material testing. We have seen that it is possible to extract important material data by performing such tests. In the next chapters we will investigate dynamic test methods.

6 DYNAMIC MATERIAL TESTING

We have seen that the static material properties can be measured by squeezing or stretching the relevant piece of material. In penetration mechanics the load on the materials will not be static, in fact it will be very dynamic, changing rapidly with time. An important question is then whether the materials have the same properties under dynamic loading as under static loading.

If the answer was yes, the world would have been much simpler. Unfortunately, for many materials, the answer is no. For example, some materials may appear harder under dynamic loading. The constitutive laws for such a material will be more complicated and will have to involve the strain rate tensor $\dot{\epsilon}_{ij}$.

Unfortunately, measuring such dynamic material properties is quite difficult. Still, we shall here attempt to describe some of the techniques that are available.

6.1 Dynamic loading

Dynamic loading of a material is a much more complicated process than static loading. Whereas in a quasi–static process, the material is loaded so slowly that a static stress state is achieved inside at all times, a dynamic process is characterised by wave propagation.

To first get a feeling of what goes on inside a dynamically loaded material, we will start our discussion by performing a numerical simulation of such a situation, using the hydrocode Autodyn. More precisely, we will examine a situation where a steel cylinder (”projectile”) impacts a “target” cylinder of the same diameter. The geometry, which is shown in Figure 5.1, has been chosen for a specific purpose of illustration.

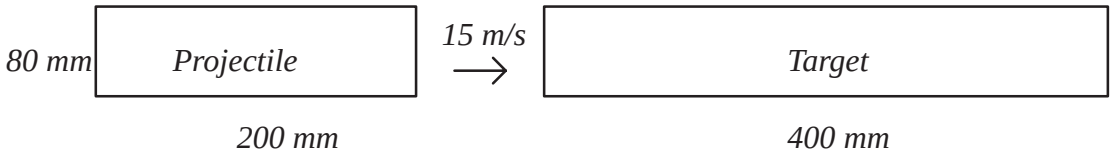

Figure 6.1 Impact geometries to be analysed.

In order to make the problem easier to analyse, the material model for the target is completely elastic. For the elastic parameters we have chosen values roughly similar to one particular type of High Performance Concrete (HPC). Thus, we have:

Density:	3000 kg/m^3
E–modulus:	36.7 GPa
Poisson ratio:	0.222

For the projectile, a traditional Mises steel model has been used. The impact velocity was 15 m/s. This should generate a square pulse in the target on impact.

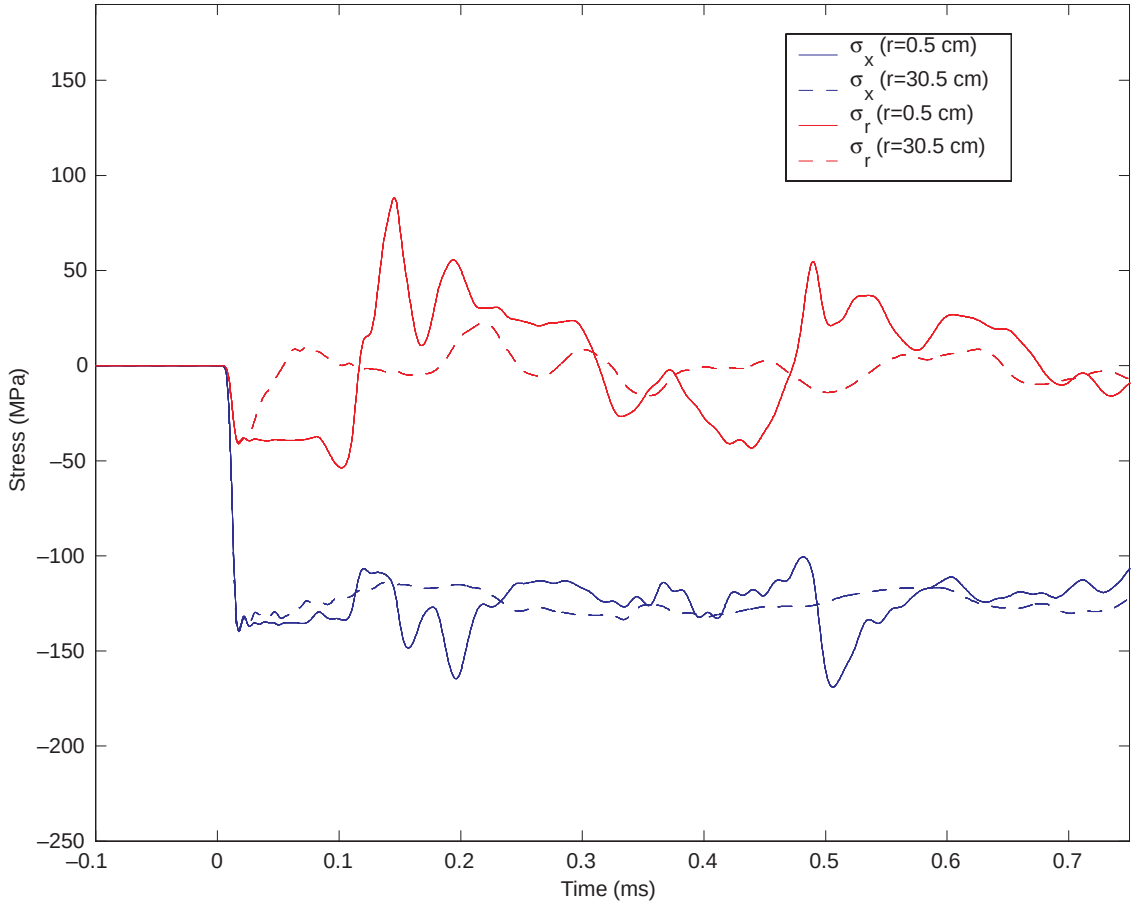

Figure 5.2: Axial and radial stress as a function of time at two points inside the target.

Our main interest was monitoring the stresses inside the target. We therefore defined "target points" at varius distances from the cylinder axis, all located 25 mm from the impact surface of the target but at different distances from the symmetry axis.

In Figure 5.2 we have plotted the axial stress (σ_x) and radial stress (σ_r) as a function of time at two different target points.

On a first glance at Figure 5.2, perhaps the most apparent thing is that σ_r appears to oscillate around zero, while the axial stress σ_x oscillates around some finite value. In particular, this is true for the target point further away from the symmetry axis. If the oscillasions had not been present, this would have very much looked like a state of uniaxial stress. In fact by averaging the stress over a longer period of time, one would expect to obtain roughly such a stress state.

However, let us look more closely at the stress state right after impact, i.e. roughly $t < 0.12$ ms, and concentrate on the target point close to the axis. In this (short) period of time, both the radial and axial stress appears to be "in phase" and roughly constant. This is different from later times where there appears to be little correlation between σ_x and σ_r. Apparantly something special is going on there. To investigate further, in Figure 5.3 we have zoomed in on this time period and plotted the ratio $\frac{\sigma_x}{\sigma_r}$ for three different target points.

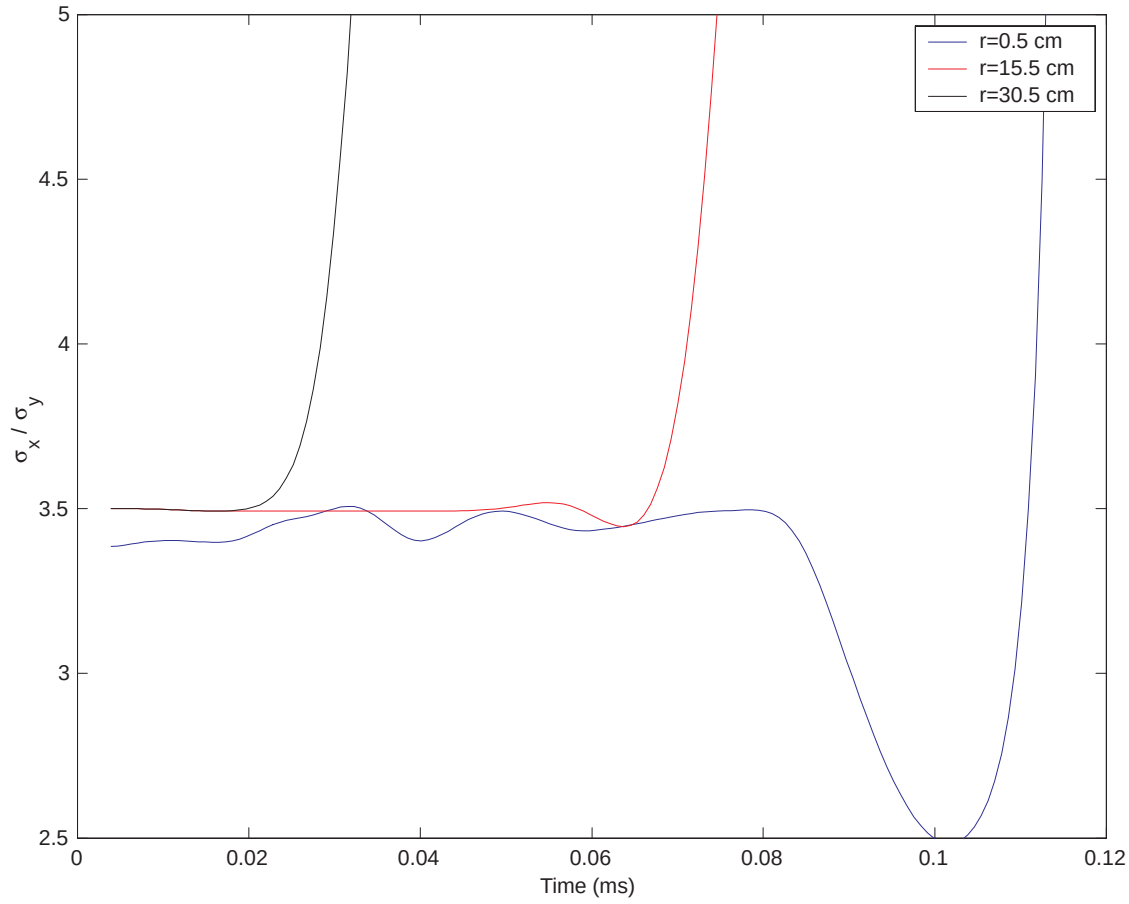

Figure 5.3: Ratio of axial and radial stress for several targets points located at different distance from the symmetry axis.

The result is very interesting. It appears that the initial ratio is around 3.50 for all the target points. Especially the two target points furthest away from the symmetry axis show a ratio that is very constant for a while until it suddenly increases. For the target point near the axis, there are some low amplitude oscillations around the same value, but the state lasts for somewhat longer.

But what is this mysterious ratio of 3.50? Where does this number come from? Why is the ratio constant early in the process? A clue to this can be found in the description of a static uniaxial strain state in Chapter 2. In Equation (2.5) we had an expression for the stresses as a function of the strain. Using this to calculate the ratio between the components, we obtain:

$$\frac{\sigma_x}{\sigma_r} = \frac{1-\nu}{\nu} \tag{6.1}$$

Now, inserting the value of $\nu = 0.222$ for the target material gives us a ratio of 3.50 for a static uniaxial strain test, which is exactly the same which was obtained during the dynamic loading process.

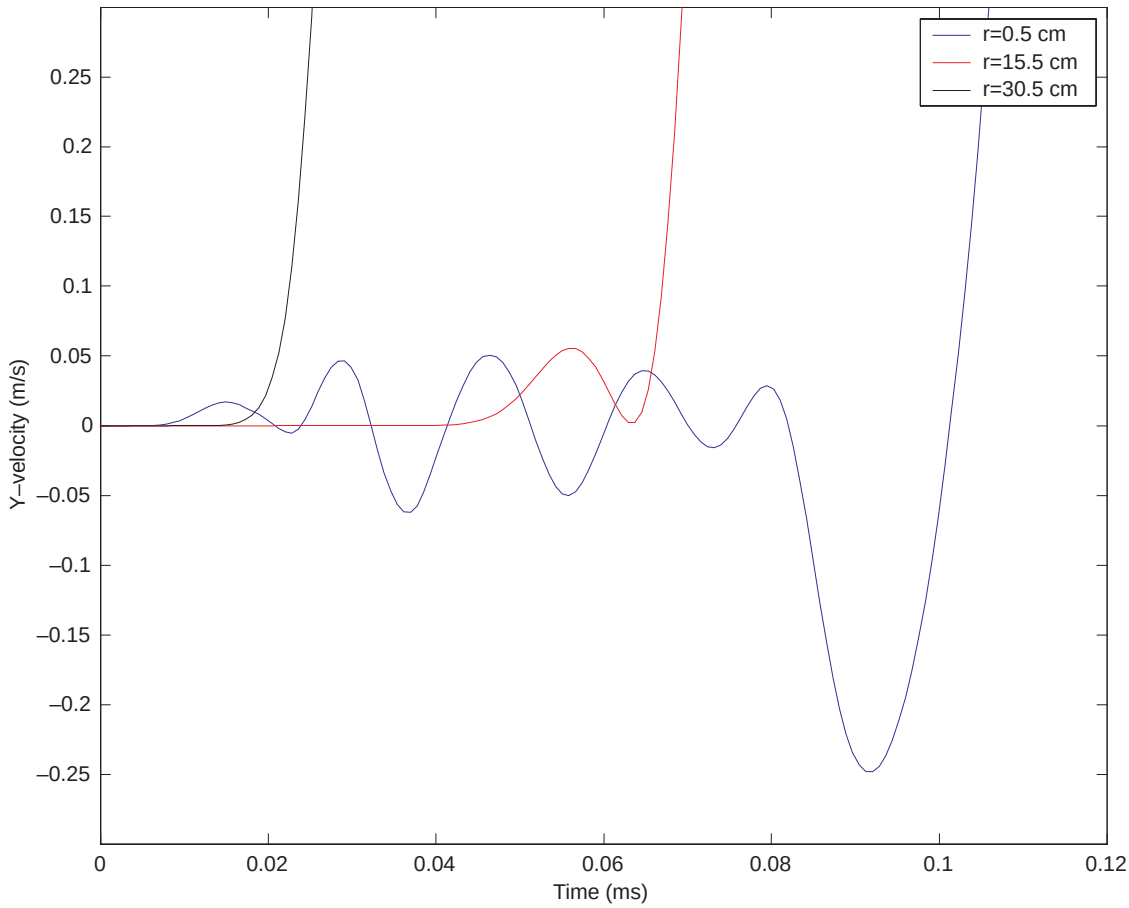

Figure 5.4: Radial velocity for the same three target points.

Thus, apparently the dynamic stress state is very similar to static uniaxial strain in the beginning, but later on it more resembles a state of uniaxial stress. Moreover, the points which are closer to the axis experiences the uniaxial strain conditions for a longer period of time. How can we explain all of this?

Let us first check out one thing. If the dynamic stress state is really uniaxial strain, the target material should be confined in some way, which means it should have no radial velocity. In Figure 5.4 we have plotted the radial velocity for the same period of time, and we see that this is indeed the case. The graphs in Figure 5.3 and 5.4 are seen to be have very similar characteristics, implying a strong connection between zero radial velocity and constant stress ratio. It seems that as long as the material is not moving radially (i.e. is confined in the radial direction), the stress state is uniaxial strain.

The following physical picture then emerges: When the impact wave travels through the material, the material wants to expand radially. However, this is not immediately possible because it is kept in place (confined) by material outside. However, the material on the boundary is free to move, and does so, releasing the material inside to move, and so on. Thus, a kind of “release” wave starts at the boundary and propagates inwards. Those parts of the target which have not yet been reached by this release wave, experiences uniaxial strain. This also explains why the target point near the cylinder axis experiences uniaxial

strain condtions for a longer period of time than the other points, as the release wave takes longer time to get there.

Let us try to find the velocity of this wave. On comparing the two outer target points in Figure 5.3, we find that the wave has travelled the 15 centimeters separating them in roughly 0.045 ms. This gives a wave velocity of 3330 m/s, which is in the same range as the sound velocity of the target.

What happens after the wave has finally propagated through to the symmetry axis? Well, since there is no energy dissipation the wave does not stop, but instead it continues going back and forth in the radial direction. This is the cause of the oscillations observed in Figure 5.2. Again we emphasize that if we average over a larger period of time, the stress state becomes very similar to static uniaxial stress, i.e. zero radial stress and constant axial stress.

So, clearly the dynamic loading process is much more complex than the static counterpart. Depending on the time and position, we can have either uniaxial stress states or uniaxial strain, and in addition we have waves going back and forth. However, the knowledge derived above can be exploited to create experiments that are particularly suited to what we want to measure.

Say that our interest is in the material behaviour under a state of uniaxial stress. Then, we have seen that after the short initial uniaxial strain phase, a state of uniaxial stress is reached in the material, except that release waves are going back and forth and disturbing the overall picture. If we could find a way of getting rid of the release waves, we would have achieved our goal.

Some thought shows us that this can be achieved by reducing the diameter of the target. This accomplishes two things: Firstly the waves last for a short period of time, and secondly their amplitude is smaller. A particular version of this test, to be described shortly, is called a Split Hopkinson Bar.

On the contrary, say we are interested in studying the material behaviour under conditions of uniaxial strain. In that case we are only interested in the first phase before the release waves have returned. To make this phase last as long as possible, we therefore need to have a target with a large diameter. A particular version of such a test is the so–called “Flyer Plate impact test”, which will be described later.

7 SPLIT HOPKINSON BAR

One of the most popular tools for dynamic testing is the Split Hopkinson Bar (SHB). It can be used to find the dynamic yield strength of a material. The test is said to work alright for strain rates in the range $(10^2 - 10^4)/s$. In this chapter we examine the SHB test method closely.

7.1 Introduction

A Split Hopkinson Bar (SHB) is illustrated in Figure 7.1, which shows a little piece of unknown material, hereafter called the specimen, sandwiched between two bars of a material whose properties are well known to us. This apparatus can now be used for obtaining information about the properties of the unknown material.

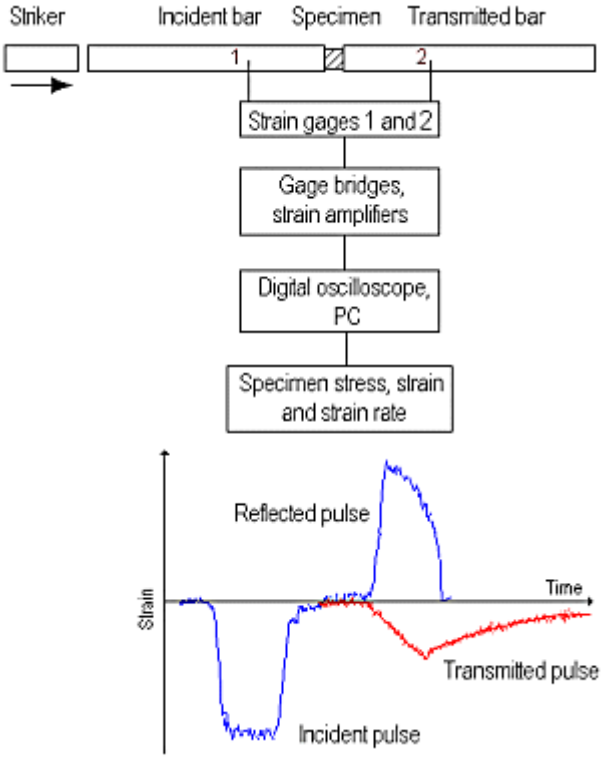

Figure 7.1: Illustration of a Split Hopkinson Bar. (Figure created by University of Tampere, Finland).

Now the experiment works this way: The first thing we do is, in some way, to create an elastic stress wave (rectangular pulse) in the left (incident) bar, for example by hitting it with a hammer, or by firing a projectile at it, or whatever. This typically generates a rectangular stress pulse in the left bar, which then travels into the specimen. There will then be a process of reflection and transmission through to the right (transmitter) bar.

From Chapter 6 we recall that when such a specimen is loaded dynamically by a stress pulse, the stress state will be close to uniaxial stress. There we examined the situation when the specimen itself was impacted, whereas in the SHB experiment things are a little bit more complicated by the presence of the two side bars.

The reason for this complication is that it enables us to stay in better control of the properties of the incoming stress wave in the specimen. This is done by measuring the strain in the left bar, and since the material properties are known, we can calculate the incoming stress amplitude. Similarly, the purpose of the right bar is to measure the outgoing stress wave from the specimen.

For measuring the strains, we have strain gauges of a suitable type attached to both the side bars, as is indicated in Figure 7.2. There might also be a strain gauge at the specimen itself. These instruments will measure the strain at their respective locations for us at all times throughout the process.

If we are to measure the strain in the left bar, it is important that the incoming and reflected pulse from the bar–specimen interface do not interfere with eachother at the point of measurement. This puts some restrictions on the initial pulse, which should be of relatively short duration compared to the length of the side bars, but of long duration compared to the test specimen (to have a long period of uniaxial stress). This means that the side bars must be much longer than the specimen, as is indicated in Figure 7.1.

We will first go through in detail what happens with reflection and transmission of waves at interfaces in one dimensional wave theory (disregarding complications such as dispersion).

If the the bars are sufficiently thin and the frequencies not too high, dispersion can be neglected, in which case the pulse can be assumed to propagate at a velocity of $c_0 = \sqrt{E_0/\rho}$ without changing its shape.

Assuming this, we shall see how the SHB apparatus can be used for measuring material data. Finally, we discuss certain practical “real–world” problems that arise in an SHB test.

7.2 Wave propagation and reflection

So, what happens when the pulse in Bar 1 eventually reaches the specimen? We shall look at this in detail. For completeness we treat both the cases of the specimen remaining elastic and when it turns plastic. It is of course the latter case which is relevant to the Split Hopkinson Bar experiment.

7.2.1 Elastic specimen

In Teland (1), reflection of elastic waves at the interface between two materials was discussed. It was shown that some part of the incoming wave would be reflected while the rest would be transmitted. The magnitude of the reflected and transmitted amplitudes depended on the surface area and relative impedance ρc of the two materials. The exact expressions were given by:

$$\frac{\sigma_T}{\sigma_0} = \frac{A_1}{A_2}\left(\frac{2R}{1+R}\right) \quad , \quad \frac{\sigma_R}{\sigma_0} = \left(\frac{1-R}{1+R}\right) \quad , \quad R = \frac{A_2\rho_2 c_2}{A_1\rho_1 c_1} \tag{7.1}$$

So, Equation (7.1) answers the question of what happens at the interface between Bar 1 and the specimen. The transmitted pulse now travels through the specimen until it reaches the interface with Bar 2, where some of it is transmitted while the rest is reflected back through the specimen. The expressions for the reflected and transmitted amplitudes are the same as given by Equation (7.1), except that material 1 and 2 are now interchanged.

But we are not yet finished: The reflected pulse now travels back to the interface with Bar 1 where it is partly reflected and transmitted, and so on.... In the end we can calculate the asymptotic stress state inside the specimen by summing the following geometric series, containing contributions from infinitely many reflections at the boundaries with Bar 1 and Bar 2.

$$\sigma_{specimen} = a\sigma_0\left(1 + b + b^2 + b^3 + ...\right) = \frac{a\sigma_0}{1-b} = \left(\frac{A_1}{A_2}\right)\sigma_0 \tag{7.2}$$

$$a = \frac{A_1}{A_2}\left(\frac{2R}{1+R}\right) \quad , \quad b = \frac{R-1}{R+1} \tag{7.3}$$

After performing similar calculations for Bar 1 and Bar 2, the final results are seen to be:

$$\sigma_{ref} = 0 \quad , \quad \sigma_{trans} = \sigma_0 \quad , \quad \sigma_{specimen} = \frac{A_1}{A_2}\sigma_0 \tag{7.4}$$

So, after a while there is apparently no reflected wave and the transmitted amplitude is equal to the incoming amplitude. The stress amplitude in the specimen is larger than the incoming amplitude (since $A_1 > A_2$ usually).

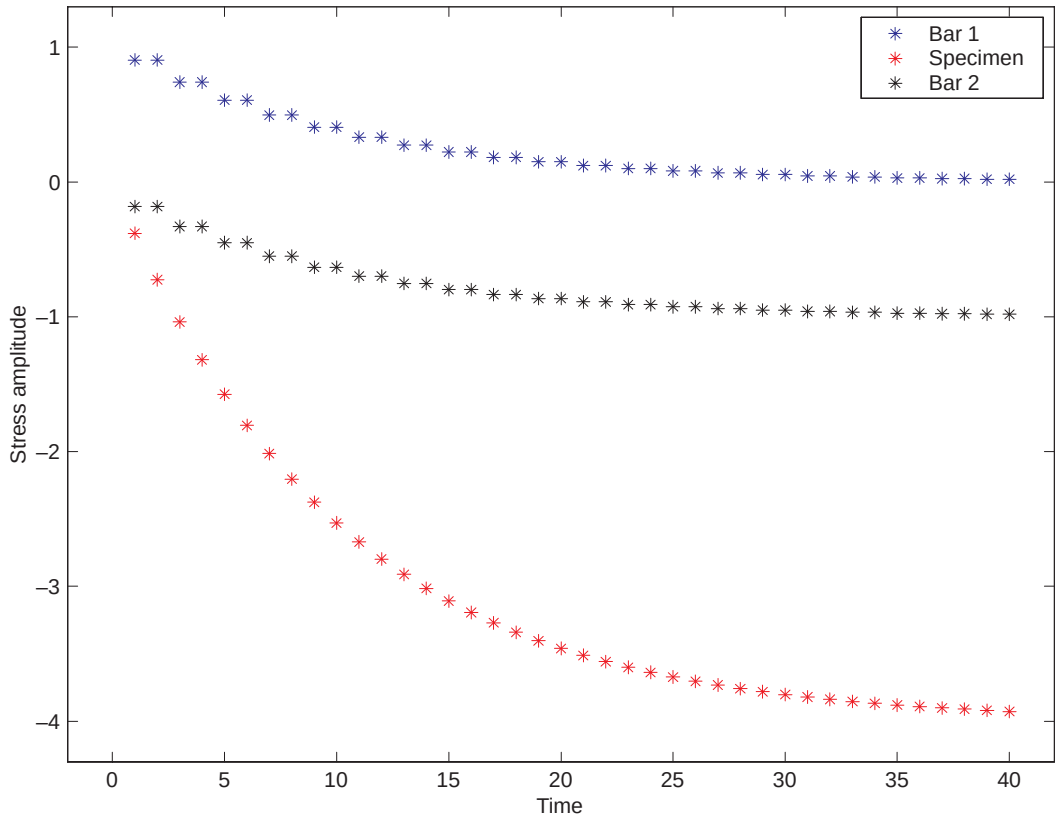

Figure 7.2: Stress amplitude as a function of time for an incoming stress pulse of amplitude $\sigma_0 = -1$. *One unit on the time scale is the time it takes the wave to travel through the specimen.* $A_1/A_2 = 4$, $R = 0.2$

One may wonder why asymptotically nothing appears to be reflected into Bar 1. The reason is that the initially reflected tensile wave is (asymptotically) exactly cancelled by the transmitted compressive stress waves that have gone through the specimen various times.

In Figure 7.2 we have shown how the stress eventually reaches its asymptotic state. Note that the total stress at a specific location in Bar 1 will be the sum of the reflected wave from the specimen and the incoming wave.

However, above it has been assumed that everything remains elastic. Since the stress is much higher in the specimen during the SHB–test, and it also probably has lower yield limit than the side bars, it is the yield limit of the specimen which determines the validity range of the calculations above.

7.2.2 Plastic specimen

In a real SHB experiment the specimen turns plastic which means that Equation (7.4) is no longer valid. Let us therefore first examine the general case of an incoming wave reaching the interface between two different materials.

In fact, this turns out to be much simpler than the elastic case. At the interface we still have the conditions of force equilibrium and velocity continuity. However, in contrast to the elastic case, we must have $\sigma_r = Y$ in the specimen since this is the highest possible uniaxial stress in a plastic material. The equations then become:

$$A_1(\sigma_0 + \sigma_r) = A_2 Y \quad , \quad v_0 - v_r = v_t \tag{7.5}$$

The solution is as follows:

$$\sigma_r = \frac{A_2}{A_1} Y - \sigma_0 \quad , \quad \sigma_t = Y \tag{7.6}$$

$$v_t = \frac{2\sigma_0 - \frac{A_2}{A_1} Y}{\rho_1 c_1} \quad , \quad v_r = \frac{\sigma_0 - \frac{A_2}{A_1} Y}{\rho_1 c_1} \tag{7.7}$$

Finally we must examine the opposite case of a plastic stress wave travelling from a material with low yield limit to a material with high yield limit. Assuming that the impedance in the second material is greater than in the first material, we realize that there can be no reflection at all because the plastic stress would then increase above the yield limit. Consequently, we have:

$$\sigma_r = 0 \quad , \quad \sigma_t = \frac{A_1}{A_2} Y \tag{7.8}$$

Returning to the SHB–experiment, we see that when the wave goes from Bar 1 to the specimen, reflection and transmission will be according to Equation (7.6) and when the wave goes from the specimen to Bar 2 there will be complete transmission as in Equation (7.8).

This means that after the front of the square pulse has propagated through the specimen, and until the rear end of the pulse reaches the specimen, we have a uniform stress equal to

the yield stress throughout the specimen. Obviously this is very different from the elastic case illustrated in Figure 7.2.

7.2.3 Brittle specimen

In the preceeding sections we looked at the SHB for both an (ideally) elastic and an (ideally) plastic specimen. However, brittle materials such as concrete present us with new challenges. This is a result of such materials exhibiting complex plastic behavior including damage evolution, pressure–dependent yield strength and time–dependent internal microcracking. Further, often (like for concrete) the material is not homogenous.

In an elastic specimen, we saw that there had to be huge amount of reflections to obtain a steady state in the specimen, whereas for an ideal plastic material, this happened very quickly. For a brittle material, practical experience shows that there will be some reflection at the interface between the specimen and Bar 2, but that after a few reflections the stress is almost uniform.

7.3 Interpretation of the SHB experiment

Let us assume that we have managed to set up an SHB experiment. Using the knowledge gained about wave reflection and transmission from the previous chapter, we shall now see how strain measurements in the two side bars can be used to generate material data for the specimen.

Let us denote the amplitude of the incoming, transmitted (through to the right bar) and reflected stress wave (in the left bar) by σ_i , σ_r , σ_t. The corresponding strains are called ϵ_i , ϵ_r , ϵ_t.

Our objective is to find a relation between stress and strain in the test material. The strain there can either be measured directly, or calculated indirectly. For practical reasons, most people calculate the stress indirectly through strain measurements in the side bars. However, TNO has been able to build a set–up for measuring the strain directly from the specimen.

Here we will examine the theory based on indirect strain measurements in the transmitter bars, and see how the corresponding stress σ and strain in the specimen can be found.

To find this we need to assume that the test material is in equilibrium with the side bars.

$$A\sigma + A\sigma = 2A\sigma = F_1 + F_2 \tag{7.9}$$

where F_1 and F_2 are given by:

$$F_1(t) = A_0 E_0 (\epsilon_i + \epsilon_r) \tag{7.10}$$

$$F_2(t) = A_0 E_0 \epsilon_t \tag{7.11}$$

Since $F_1 = F_2$ because of the equilibrium assumption, we have finally:

$$\sigma(t) = E_0 \frac{A_0}{A} \epsilon_t(t) \tag{7.12}$$

If, for some reason, we do not measure the strain in the test material directly, this quantity can also be estimated from measurements on the side bars. Let $V_1(t)$ and $V_2(t)$ be the velocity of the interfaces. Then the (assumed uniform) strain rate in the test material is given by:

$$\frac{d\epsilon}{dt} = \frac{V_1 - V_2}{L} \tag{7.13}$$

The velocities are also calculated indirectly from strain measurements in the side bars. From Equation (4.26) in (1) we have:

$$V = c_0 \epsilon \tag{7.14}$$

and thus:

$$V_1 = c_0(\epsilon_i - \epsilon_r) \quad , \quad V_2 = c_0 \epsilon_t \tag{7.15}$$

giving us:

$$\frac{d\epsilon}{dt} = \frac{c_0}{L}(\epsilon_i - \epsilon_r - \epsilon_t) = -2\frac{c_0}{L}\epsilon_r \tag{7.16}$$

where we have used the equilibrium condition to obtain the second equality. Now the strain rate can be integrated over time to give us the strain itself.

7.4 Tensile behaviour

There are variations of the SHB–test with which we can measure tensile behaviour as well. We won't go into details about this, except to draw the attention to some of the possible experimental set–ups which are shown in Figure 7.23

In one of these set–ups, a "collar" lets the initial compressive pulse bypass the specimen before it reflects at the free surface and returns as a tensile pulse. Yet another method is shown in (d) where a striker tube is used instead of a striker bar.

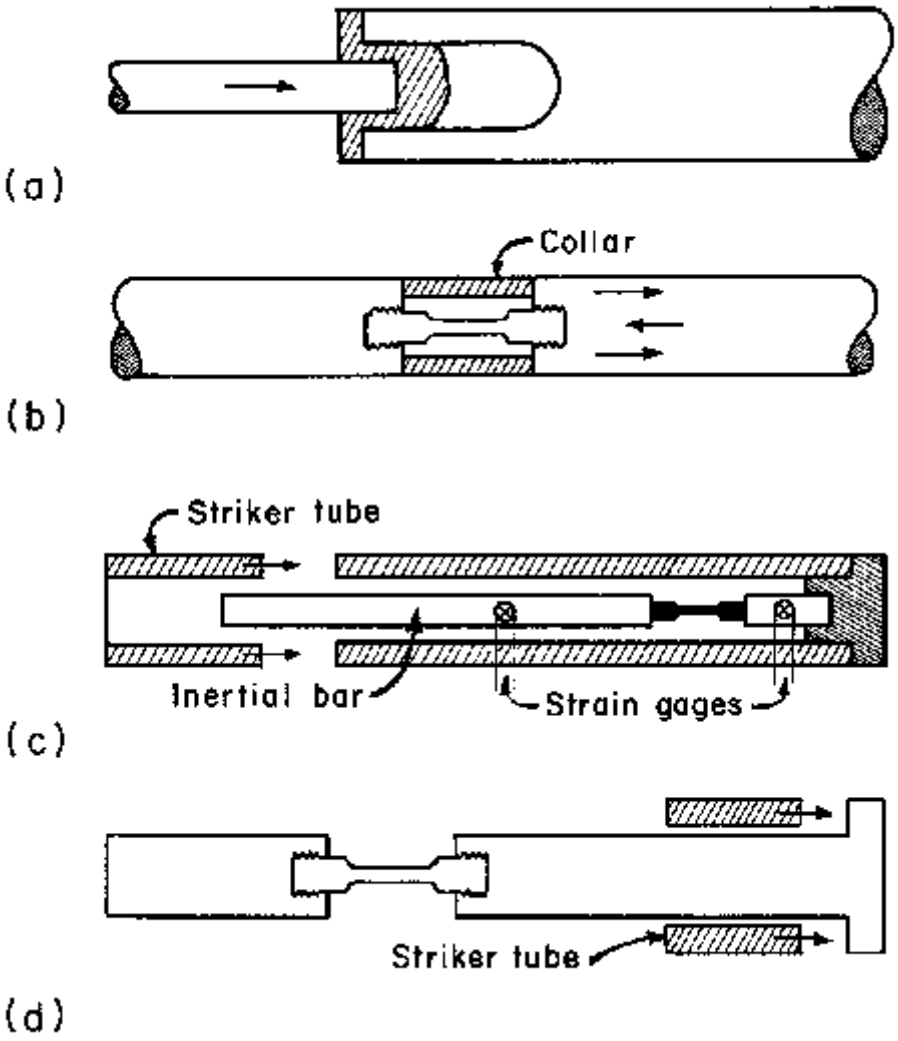

Figure 7.2: Various set–ups for tensile tests using the SHB technique. Figure taken from (8).

7.5 Results from a Split Hopkinson Bar test

Ideally, a material test should provide us with complete data for all stress components σ_{ij} as functions of the strains ϵ_{ij} and strain rates $d\epsilon_{ij}/dt$. We see that the output from Split Hopkinson Bar experiments is the stress σ_x as a function of the strain ϵ_x and the strain rate $d\epsilon_x/dt$, so it is not quite everything we want. The question is whether this information is of any use to us.

Let us assume that the stress state in the specimen during an SHB experiment can be regarded as pure uniaxial stress. If the specimen has a yield limit which is independent of pressure (like a von Mises or Tresca material), we can easily read the yield limit from the one–dimensional stress–strain curve obtained from the experiment.

By performing several experiments with different amplitudes on the initial stress waves, we can vary the strain rate and examine whether the yield limit is strain rate dependent.

Such information can not be obtained from quasi–static experiments (although the yield limit could easily be found from such an experiment), so this is one use of the Split Hopkinson Bar.

However, we are primarily interested in testing materials like concrete where the yield limit depends on the pressure (Mohr–Coulomb, Drucker–Prager type). In this case yielding is described by a yield curve (surface) and not a single point (yield limit). The SHB–test can only provide data for one point on this curve since the specimen is always loaded in uniaxial stress (at least we are assuming this to be the case).

For this point on the yield curve, the same conclusion holds that we can investigate the strain rate dependence by varying the initial stress. If we know the quasi–statical yield curve from other experiments we can also make the assumption that all other points on the curve have the same strain rate dependence (or some other assumption) and estimate the strain rate dependence of the whole yield curve.

By using very small specimens of around 1 mm, strain rates up 10000 have been achieved. However, to use such small specimens the material has to be very homogenous, which can not be said about concrete. A concrete specimen would at least have to be several centimeters for the test to have any meaning, and this again limits the achievable strain rates in such a test. Therefore, the maximum strain rate for concrete will be much lower.

7.5.1 Possible improvements on the SHB test

More information could be obtained from the SHB–test if the specimen was confined in some way. If the confinement pressure could be varied, the specimen might follow different paths in stress space and provide us with data for more than one point on the yield curve.

There are, however, major practical problems with getting useful data from a confined Split Hopkinson Bar. DERA tried this but had problems with waves in the confining material. However, Gary et. al (9) apparently have a working version of the confined SHB, though.

Bhushan/Jahsman (10) almost achieved a state of uniaxial strain in a similar setup, but had problems with the yield limit being much higher in uniaxial strain than in uniaxial stress. However, these guys were testing metals and not concrete, and it is unlikely that the yield stress would ever be higher in concrete than in steel (or whatever material the side bars are made of) no matter what confinement we have.

The advantage of the SHB experiment seems to be that we can obtain information about the effect of strain rate on the yield limit of the material. Apparently we can not use the SHB to obtain the constitutive relations at higher stresses than in quasi–static tests. We are limited by the yield limit of the material in the side bars.

7.6 Practical problems with the SHB

So far we have described an “ideal” Split Hopkinson Bar test. However, in the real world, several practical problems arise. Here we will briefly describe some of these problems and how they can be dealt with.

7.6.1 Friction

Our first problem is friction at the interface between the specimen and the two side bars. As a result of this friction, there will be a force preventing the specimen from expanding radially. However, this force works only at the interface and not inside the specimen, so the inside is able to expand freely. This results in the specimen obtaining a socalled “barrel” shaped form.

This effect will have influence on the wave propagation in the specimen, as the wave will now pass through a bar with non–constant cross–section area. The amplitude of the wave will then be reduced where the radius is large compared to where the specimen radius is small.

It is therefore very important to eliminate/reduce friction between the bars. By applying a thin film of lubricant at the interfaces, this frictional constraint can be greatly reduced, however.

7.6.2 Dispersion

Another potensial problem with the SHB is dispersion of the wavepulse. So far we have assumed the incoming pulse to propagate through the bars without changing shape, but this is actually only an approximation.

As described in Teland (1), on solving the equations for wave propagation in a bar it is found that the propagation velocity depends slightly on the frequency of the wave. Consequently, a pulse consisting of waves with many different velocities, will not be able to retain its original shape. Obviously this might lead to problems with measurements in the SHB experiment. Dispersion is, in particular, a problem for rectangular pulses which we know are composed of waves at infinitely many frequencies at different amplitudes.

It is beyond the scope of this report to look at dispersion in detail. However, the reason that dispersion appears is that the Poisson effect makes the bars expand/contract radially, altering the stress distribution so that the stress is not constant over a cross section of the bar. The amount of dispersion depends on the frequency of the waves and the radius of the bar. For a given radius this will put an upper limit on the allowable frequencies before the pulse becomes too distorted. Since the strain rate is directly related to the frequency, this implies that there is a maximum strain rate as well.

There are several ways to deal with the problem of dispersion.

One method is to theoretically account for that the measured strain as a function of time has been slightly distorted by dispersion. If the dispersion characteristics of the material is known, it it possible to mathematically process the measured results to find what the measurements would have been like if no dispersion had been present. It is probably a good idea to experimentally determine the dispersion characteristics of the transmitter bars, instead of only performing theoretical calculations. More details about such an experimental procedure can be found in (11).

In Forrestal (3) the dispersion effects were reduced by increasing the rise time of the pulse, so that the the stress increased (approximately) linearly as a function of time. In practice this was achieved by placing a small piece of material between the striker and input bar, in this case a thin copper disk. A gradual build–up of stress from stress components that are transmitted after reflections at the copper–bar interface, just as described earlier for the Bar 2–specimen interface, is then obtained.

An even more sophisticated method is to generate a pulse consisting of only one frequency. This can be accomplished by having a projectile that has been carefully shaped. It has been shown in (7) that a half sine wave may be generated by this approach. We shall soon see that there are other advantages to creating such an impact pulse, as well.

7.6.3 Fracturing of the specimen

Another potensial problem arises for brittle materials. If the incoming wave gets dispersed, the low frequency components will arrive at the specimen first. If the amplitude of these components is comparable to the strength of the specimen, the specimen might fracture before the main part of the pulse has entered it. The measurements will then subsequently not provide any useful information.

Again, this problem can be solved by creating an incoming pulse which does not disperse.

7.6.4 Pulse alignment

Yet another, more technical, problem involves the simultaneous measurement of strain in the two transmitter bars. Obviously, it is important that these two quantities are really measured at the same time. Apparently, it is not trivial to determine the “first point” in a pulse. However, there exist special numerical techniques for aligning the first point in both pulses, without needing assumptions like perfect bar–specimen interface and known velocity in the specimen.

7.7 Conclusions

We have now seen how the Split Hopkinson Bar experiment works. The specimen is loaded in (roughly) uniaxial stress for a (relatively) long period of time, and material data are generated from measurements on the transmitter bars.

In the next chapter we shall examine the Flyer plate test, which is more similar to the impact situations described in Chapter 6. It is of shorter duration so that the material properties are measured in uniaxial strain.

8 FLYER PLATE TEST

In this chapter we will describe the Flyer plate test. However, in order to understand the theory behind this test, it is necessary to look more in detail at the impact process.

8.1 Impact

Let us re–examine the familiar situation from Chapter 6, where one plate impacted another plate of a different material. Because of symmetry we will work in cylindrical coordinates with our coordinate system oriented so that impact is in the x–direction.

We have learned that right after impact a release wave starts propagating in from the boundary, enabling the material to start expanding radially. However, those parts of the material which have not yet been reached by this wave will be in a state of uniaxial strain. Obviously the material along the symmetry axis will retain this state for the longest duration of time, and will therefore be of special interest to us.

The particles in this part of the material will have obtained some velocity in the x–direction, which we denote by U_p (the index indicates that this is the particle velocity and not the wave velocity). By studying elastic impact, in Chapter 5 we showed that the stress state was of uniaxial strain, but we made no attempt at determining U_p or the stress components σ_x and σ_r as a function of impact velocity. This is the subject of the current section.

Whereas we in Chapter 5, for illustration purposes, only looked at a purely elastic situation, this time we will consider an elastic–plastic problem. However, we add the assumption that conditions are so that a plastic shock wave is generated in both the projectile and the target. As was shown in Teland (1), for this to happen, it is necessary that materials have a stress–strain curve whose slope (which determines the wave velocity) increases with stress.

For a sufficiently high stress, the slope may even become larger than the elastic slope, so that no elastic precursor wave is generated and only a single shock wave is formed. This simplifies the problem because we do not need to deal with a complicated two–wave elastic and plastic wave structure.

8.2 Equation of state

Before continuing we have to say a few words about the concept of Equation of State (EOS). Usually an EOS means an equation relating the pressure to the density and possibly other “state variables” such as temperature etc.

However, in shock physics/dynamic experiments, people usually mean a relation between the shock velocity U_s and the particle velocity U_p when they talk about an EOS. This is (probably) because these are the quantities which are measured in such experiments. Such

a relation can, however, be used to derive a relation between the pressure and density so that everything looks familiar.

Let us imagine that a shock wave is propagating with some given velocity U_s in our material. The relationship between the material state behind and in front of the shock wave is given by the shock equations, which are basically the conservation equations across the shock front. Ignoring temperature effects, we only need the equations for conservation of mass and momentum to describe the system:

$$\rho_0 U_s = \rho(U_s - U_p) \tag{8.1}$$

$$\sigma_x = -\rho_0 U_s U_p \tag{8.2}$$

Here we have used that the pressure in front of the shock front is zero. Notice the product $\rho_0 U_s$ which appears in both equations. This quantity is referred to as the (shock) "impedance" of the material, often denoted by *Z*. It is analogous to the elastic impedance which is given by $\rho_0 c$. However, whereas the elastic impedance is constant, the shock impedance will turn out to be a function of particle velocity.

The density ρ in the "shocked region" can also be expressed as a function of the strains. In our case, there are only strains in the x–direction, so we have:

$$\rho = \frac{\rho_0}{1 + \epsilon_x} \tag{8.3}$$

The two equations (8.1)–(8.2) have three unknowns: σ_x , ρ and U_p. Thus, one equation is missing if we want to find a solution. However, this is not surprising since we have not said anything about the properties of the material, but only assumed conservation of mass and momentum.

The missing equation therefore has to be the constitutive law which tells us how the material behaves. Typically, this is a relation between stresses and strains. However, mathematically a relation between the shock velocity and particle velocity $U_s = U_s(U_p)$ will turn out to be equivalent.

Let us assume that for our material such a relation is measured experimentally to be linear on the following form (which is typical for metals):

$$U_s = c_0 + SU_p \tag{8.4}$$

where c_0 is the elastic wave velocity and *S* is a positive constant. The velocity of the shock wave is thus greater than the elastic velocity, as was assumed initially.

Now, Equations (8.1)–(8.4) can easily be solved and the pressure as a function of density can be found:

$$\sigma_x = \frac{\rho_0 c_0^2 \epsilon_x}{(1 + S\epsilon_x)^2} = \frac{(K + \frac{4}{3}G)\epsilon_x}{(1 + S\epsilon_x)^2} \tag{8.5}$$

where we have used that the elastic wave velocity is calculated in uniaxial strain. Equation (8.5) is the conventional form of an equation of state, but it is now clear that an expression on the form of Equation (8.4) is just as good. Note that for a compressive wave, both the stress σ_x and the strain ϵ_x are negative, resulting in increased stress for large strains.

In Figure 10.2 we have plotted Equation (8.5) for various values of the parameter *S*. It is seen that as *S* grows larger, the stress corresponding to a particular value of strain increases as well. This is consistent with the increase of the shock velocity for growing *S*, as follows from Equation (8.4). Note that for *S=0*, the shock velocity is equal to the elastic wave velocity and Equation (8.5) consequently reduces to the elastic uniaxial strain expression.

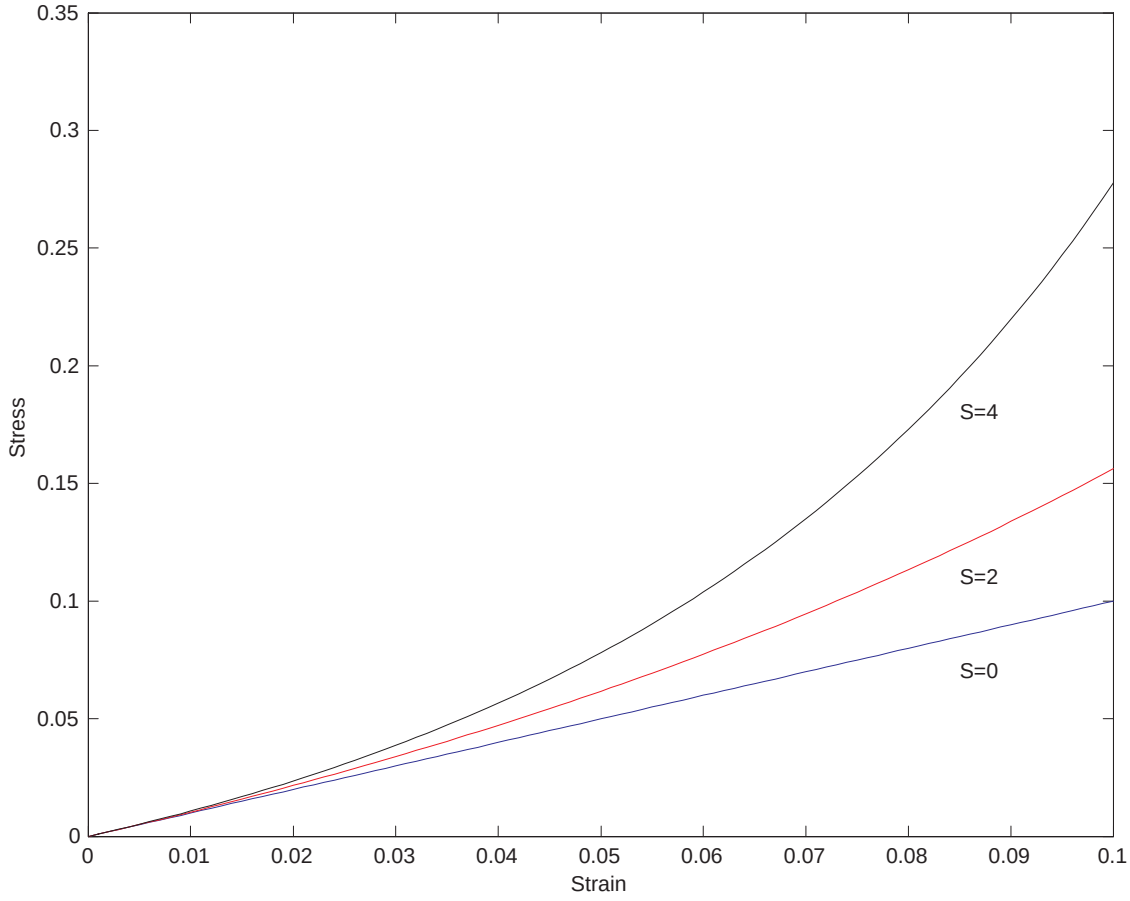

Figure 8.1: Stress–strain relationship for different values of the parameter S in the (linear) EOS Equation (8.4). Note that the stress is divided by $\rho_0 c^2$ *and that actually the negative of stress/strain has been plotted (thus, positive values in the figure corresponds to compression).*

Finally, we can calculate the radial stress σ_r . Since the material is plastic, it can be found from the yield condition after we have found σ_x. Assuming a Mises or Tresca yield condition, we have:

$$\sigma_x - \sigma_r = Y \tag{8.6}$$

Note that if the stress components are much larger than the yield limit *Y*, they have to be almost equal according to Equation (8.6). In this case, the material behaves approximately

as a fluid, where all stress components are the same and there are consequently no shear stresses.

Equation (8.5) was derived on the assumption of a linear relation between shock velocity and particle velocity. For a more general relation $U_s = U_s(U_p)$, this equation does not hold, but a relation between pressure and density will always be possible to derive.

Our problem of experimentally finding the EOS of an unknown material is then reduced to measuring the relationship between particle and shock velocity for that particular material. Let us now see how σ_x and U_p can be calculated for an impact situation.

8.3 Calculating pressures and particle velocities

Now we want to find out exactly what happens inside the two materials after impact, but before the release wave arrives. The situation in the plates/bars right are illustrated in Figure 8.2. Plate 1 has come in from the left with an impact velocity denoted by V_0. After colliding with plate 2, shock waves have started propagating inside both plates.

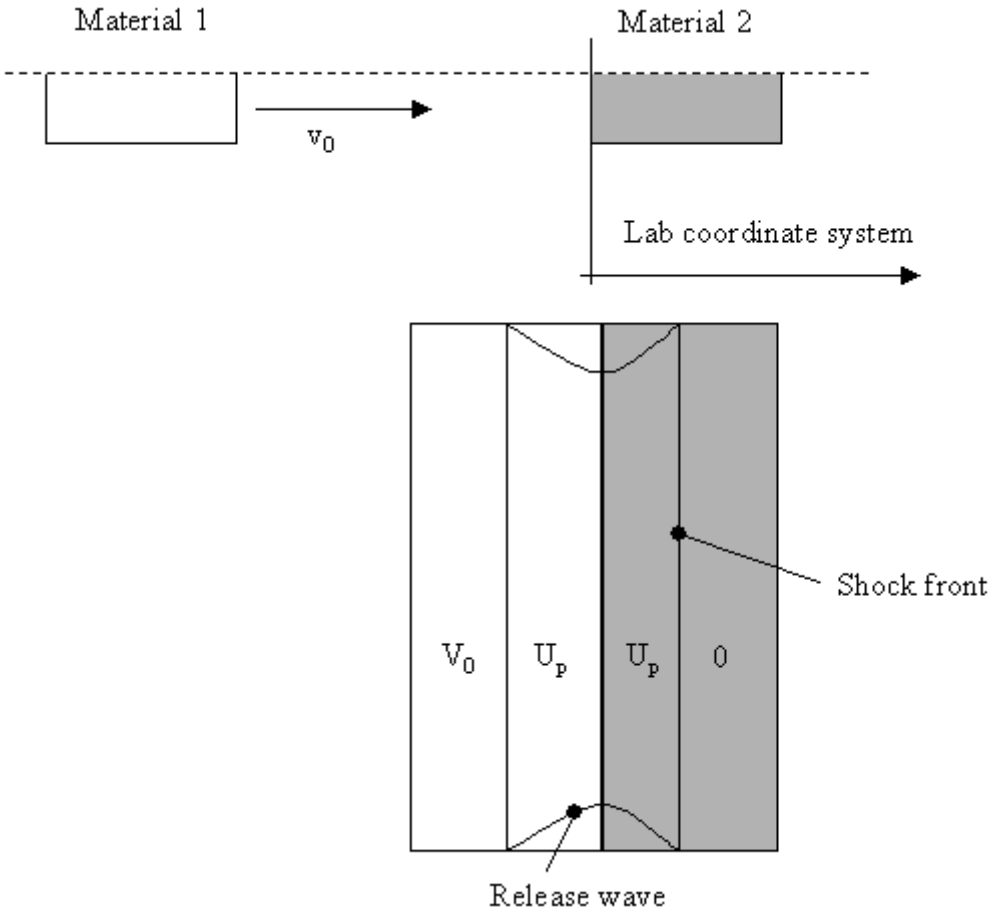

Figure 8.2: Illustration of the impact dynamics of a Flyer plate test.

The stress and particle velocities have to be continuous across the material interface, which implies that the pressures/stresses and particle velocities behind the shock waves have to be identical in both materials.

Thus, in the region behind the shock wave, the velocity is equal to U_p and the stress is equal to σ_x. However, the shock wave is moving at different speeds in the two materials, and the difference in velocity between the disturbed and undisturbed materials are therefore $V_0 - U_p$ for the projectile and $U_p - 0 = U_p$ for the target.

Using Equation (8.2) in both plates, we have:

$$\sigma_{x1} = \rho_{01} U_{S1} U_{p1} \tag{8.7}$$

$$\sigma_{x2} = \rho_{02} U_{S2} U_{p2} \tag{8.8}$$

where U_{p1} and U_{p2} are the particle velocities *in the respective rest frame* of the plates, i.e. the frame in which the unshocked material is at rest. It is very important to realize that two plates are not at rest in the same reference frame.

For simplicity, we assume that the EOS for the two materials are linear:

$$U_{S1} = C_1 + S_1 U_{p1} \tag{8.9}$$

$$U_{S2} = C_2 + S_2 U_{p2} \tag{8.10}$$

Inserting the EOS into the shock conditions yields

$$\sigma_{x1} = \rho_{01}(C_{01} + S_{01} U_{p1}) U_{p1} \tag{8.11}$$

$$\sigma_{x2} = \rho_{02}(C_{02} + S_{02} U_{p2}) U_{p2} \tag{8.12}$$

σ_{x1} and σ_{x2} have to be equal, as mentioned earlier. But now we have to be careful: Remember that U_{p1} and U_{p2} are measured in different rest frames. Let us do our calculations in the laboratory frame, which is the same as the rest frame for plate 2.

In this fixed coordinate system, we will designate the particle velocities as U_{pA} and U_{pB}, reserving the subscripts 1 and 2 for Equations (8.7) and (8.8).

a) Target

The particle velocity U_{pB} in the compressed region is equal to the interface velocity (and of course, in planar impact situations the particle velocity relative the interface is always zero for both materials). The material ahead of the shock is at rest. Thus, $U_{p2} = U_{pB}$.

b) Projectile

The particle velocity U_{pA} in the compressed region is also equal to the interface velocity. However, the particle velocity U_{p1} to be used in Equation (8.11) should be measured relative the undisturbed projectile material, which is moving at velocity *V*. Consequently, we have $U_{p1} = V - U_{pA}$

This gives us the following relations:

$$\sigma_{x1} = \rho_1 C_1 (V - U_{pA}) + S_1 (V - U_{pA})^2 \tag{8.13}$$

$$\sigma_{x2} = \rho_2 C_2 U_{pB} + S_1 U_{pB}^{\ 2} \tag{8.14}$$

Furthermore, we have $U_{pA} = U_{pB} = U_p$ so that

$$\rho_1 C_1 (V - U_p) + S_1 (V - U_p)^2 = \rho_2 C_2 U_p + S_1 U_p^{\ 2} \tag{8.15}$$

This is nothing more than a simple algebraic equation of second degree for U_p. The solution is rather ugly, though, and is given on page 112 in Meyers (8) (beware of the two misprints and note that the explanation of the coordinate relation $U_{p1} = V - U_{pA}$ is erroneous in Meyers).

After the particle velocity U_p has been found, Equations (8.13) or (8.14) can be used to determine the stress σ_x at the impact interface.

It is important to be aware that Equation (8.15) was derived on the assumed linear relationship (8.9)–(8.10) between shock and particle velocity. Although this kind of relationship is typical for materials such as metals, it is not true in general that the EOS is linear in this way. For many materials the functional relationship between U_s and U_p might be quite different and needs in general not be linear. However, this is not really a problem for us. Although the equivalent of Equation (8.15) will look slightly different it will still only be an algebraic equation. In the worst case, where no analytic solution exists, the equation can easily be solved numerically.

This brings us to the subject of flyer plate tests, where only the properties of one of the materials is known in advance. The purpose of the test is, of course, to determine the properties of the other material.

8.4 Simple Flyer Plate experiment

There are several versions of the Flyer plate experiment, all having in common that they involve a collision between (at least) two plates, one with known properties and one whose properties are to be found.

In the simplest version of the test, a plate with known properties (the projectile) is simply impacted onto a target plate with unknown properties. This test can be used to determine the EOS of the target plate. By performing several experiments at different impact velocities, we can find out whether the EOS depends on the strain rate.

Let us see how such data can be derived from the actual measurements. The only data we have at our disposal is the particle velocity at the rear end of the target, which is measured using VISAR equipment (or similar).

Assuming that the boundary remains stress free, we find that the velocity which is measured by the VISAR is twice the particle velocity U_p behind the shock front. By measuring the time the wave needs to travel through the target plate we can determine the shock velocity U_s. By performing the experiment at different impact velocities, we can determine the relationship between the shock velocity and particle velocity. Using the methodology outlined in Chapter 8.2, we can then determine the EOS of the target plate.

This method works well for ductile materials, but unfortunately not for brittle materials. The reason has to do with inelastic behaviour during loading and unloading, which means that the particle velocity can not so easily be calculated from the measured rear velocity. More details are given in (4).

Further, for ductile materials we can also determine the dynamic tensile strength using this method. Because of the free boundary, a tensile pulse is reflected into the plate, cancelling the incoming square compressive pulse. The incoming pulse is of finite duration and eventually the material will experience a tensile stress. If this stress is above the tensile strength, we obtain tensile failure at a specific point inside the target plate. This is eventually seen as a dip in the measured rear end velocity. The dynamic tensile stress can then be determined through analysis of the dip in velocity.

8.4.1 Strain rates

It is often said that Flyer plate tests are performed at very high strain rates. This is true, but it is important to realize that, in fact, the strain rate is very small for most of the time, except when the pulse arrives, at which time it becomes extremely large for a very short period of time. Averaged over this period of time, it can be said that the strain rate is relatively large, though, but this average is not an interesting quantity.

If we are to measure the strain rate properly, it can also be derived from the VISAR measurements. By measuring $U_p(t)$, and assuming that the pulse does not change shape (at least not drastically over short distances, which is a reasonable assumption), we can apply the following identity:

$$\dot{\epsilon} = \frac{\partial v}{\partial x} \simeq \frac{U_p(x + \Delta x, t) - U_p(x, t)}{\Delta x} \tag{8.16}$$

However, a measurement at a point a distance Δx away will (assuming no change of pulse shape) give the same result as a measurement at the same point, but $\Delta t = \frac{\Delta x}{U_s}$ later. Thus, we have:

$$\dot{\epsilon} = \frac{U_p(x, t + \Delta t) - U_p(x, t)}{\Delta X} = \left(\frac{U_p(x, t + \Delta t) - U_p(x, t)}{\Delta t} \right) U_s = \frac{\partial U_p(t)}{\partial t} U_s \tag{8.17}$$

Thus, the strain rate depends on the shock velocity and the rise time of the pulse. If the pulse is perfectly square, the strain rate will be infinite for an infinitesimally short time and then zero. A real pulse will not be exactly square, but during the rise time, strain rates can reach as high as 10^7/s.

8.5 Inverse Flyer plate test

As explained in Chapter 8.4, the regular flyer plate test does not work for brittle materials. For such materials, the Inverse flyer plate test can instead be used for deriving the EOS. This test is very similar to the normal flyer plate test, but the specimen is used as a projectile instead of as a target. In addition, the specimen is supported by a thin Aluminum plate (or similar) at it's rear end. The VISAR measurements are now made on the back face of the (well known) target instead of at the unknown specimen material.

So, this time we must find the EOS without performing any measurements on the unknown material. How can we do this?

Well, the particle velocity U_p is quite simple to determine because we know that it must be equal in both materials (because of continuity conditions), so it does not matter in which material we measure.

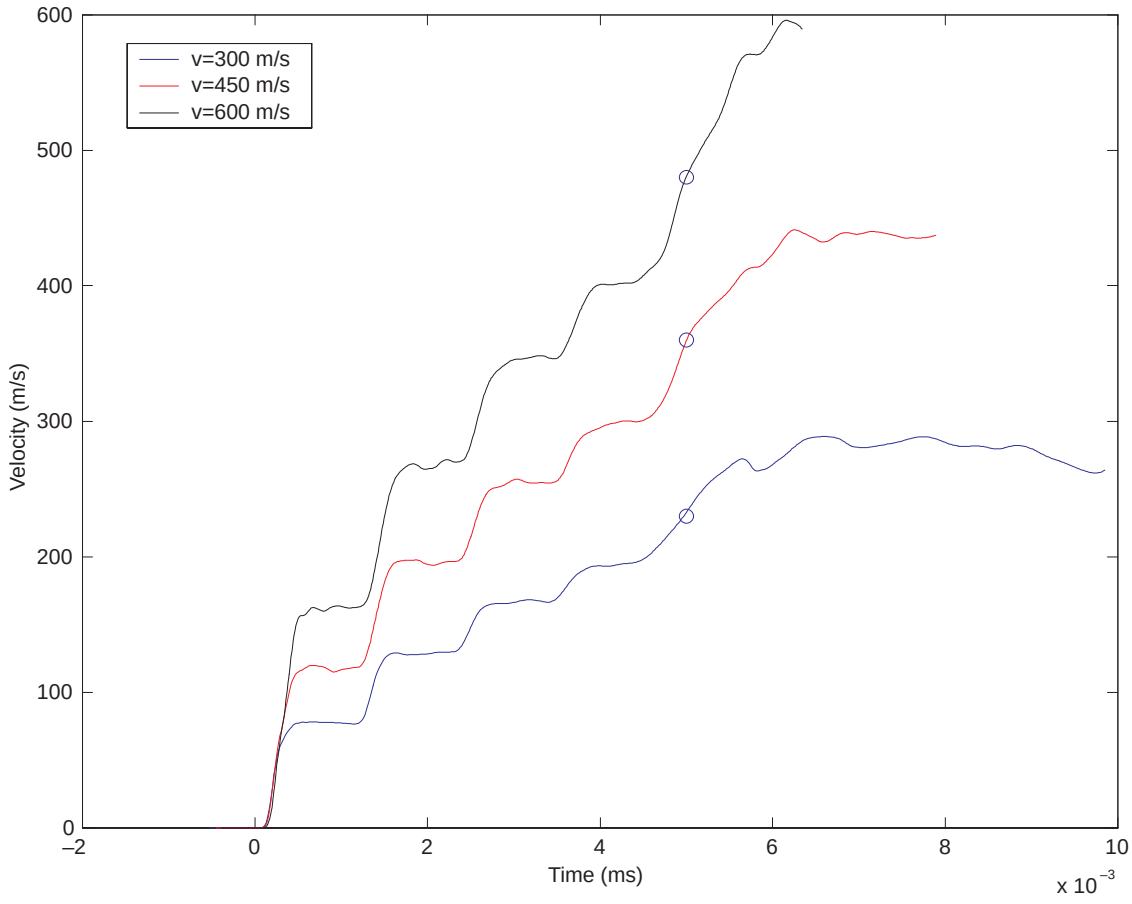

Figure 8.3: Back face velocity in an inverse flyer plate experiment with an elastic–plastic Mises material.

Further, when the wave going through the specimen (projectile) reaches the supporting Aluminium plate, it will be partly reflected as a compressive wave since Aluminium has a higher impedance. (Some of the wave will be transmitted into the Al–plate as well). The shock velocity U_s can now be measured by observing how long time it takes before the

wave reflected into the projectile (specimen) is returned to the back face of the (well known) target material. This is seen as a jump in the velocity measurement at the back face.

When the reflected wave in the steel plate is reflected as a tensile wave, it travels back until it reaches the interface with the brittle specimen, where some of it is reflected and some of it is transmitted. The part that is transmitted, travels back through the steel plate and when it reaches the boundary it results in an increase in measured particle velocity. By observing this increase we can determine how much of the wave was reflected and transmitted at the material interface, and thereby determine the concrete impedance.

Let us illustrate this procedure with the results from some Autodyn simulations of an inverse flyer plate test. First, let the specimen be a perfectly plastic Mises material, while the back plate is made of 4340 Steel. The specimen plate was 8 mm thick while the target steel plate had a thickness of 3.3 mm. Finally, the supporting Aluminium plate was 2 mm thick.

A target point was placed in the center of the rear end of the steel plate, and the velocity measured as a function of time is shown in Figure 8.3 for three different impact velocities. We notice that the velocity increases in “jumps”. The small jumps are due to the wave being reflected at the specimen interface and returning to the rear end, where it again reflects at the free surface. However, more importantly, after a while there is a much larger jump in velocity and this comes from the wave which went into the specimen and reflected at the supporting plate before travelling back through the specimen and transmitting at the interface with the back plate.

From this we can measure the shock velocity. It is a little difficult to pinpoint exactly the arrival time of the wave, but we go for somewhere around 50 μs, which has been illustrated by a circle in the figure. Appropriate error limits must of course always be included in data like this, but we will not go into this here. We note that the arrival time appears to be independent of the impact velocity of the concrete plate.

Knowing the velocity in 4340 Steel to be 5843 m/s, we find that 5.6 ms is spent in the 3.3 mm steel plate, which means that approximately 44.4 μs is spent going through 16 mm concrete. This gives a “shock” velocity of 3610 m/s, which compares well with the theoretical value of 3730 m/s, taking into consideration the difficulties with pinpointing exactly when the wave returns.

As already noted, the shock velocity seems to be independent of the impact velocity and thus the particle velocity. Consequently we conclude that the shock velocity is just equal to a constant, namely the sound velocity under uniaxial strain for this material, and S=0. Putting this into Equation (8.5) we find that this corresponds to a linear pressure–density EOS, as was expected (since the material actually has such a linear relationship).

However, let us now see what happens when the material has a different EOS. The results from such a simulation are displayed in Figure 8.4. Again it is difficult to pinpoint exactly

when the reflected wave actually arrives, but some reasonable estimates have been indicated in the figure.

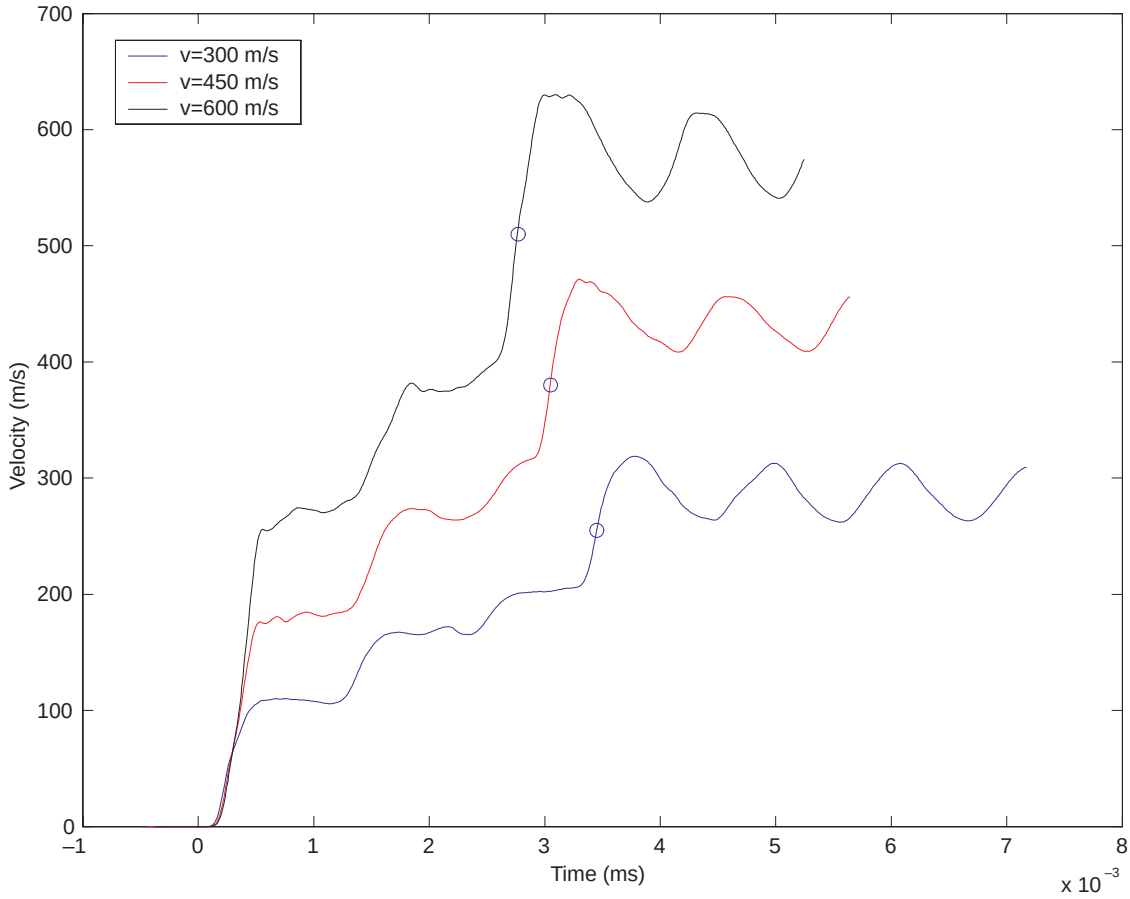

Figure 8.4: Velocity at the back face of the target plate for a material with a linear shock EOS.

However, as can be seen from Figure 8.4 there is no doubt that the arrival time is dependent on the impact velocity. Using the data for the arrival time at different impact velocities, it is now possible to calculate the EOS of the specimen.

8.6 Even more advanced flyer plate test

A problem with the inverse flyer plate test is that it does not enable you to achieve high enough pressures inside the concrete. To enable this, yet another version of the flyer plate test has been developed.

The new set–up is similar to the original flyer plate test, except that the (thin) target is backed up by another (thick) plate made of (well known) material with higher impedance. The idea is to make the pressure build up inside the specimen by having a thin specimen sandwiched between two thicker plates of higher impedance.

Now, let us closely investigate what happens after impact. Right after impact there must be continuity in velocity and stress at the interface, which leads to a shock wave going

through the target and the projectile at a specific velocity U_{p1}. Further, until the wave reaches the interface with the supporting plate, it does not yet know that the target is backed up by a support plate, so everything is exactly similar to the original flyer plate test. If we know the EOS of the target for the impact velocity (for example from doing inverse flyer plate tests), we can determine U_{p1}.

When the shock wave reaches the interface between the specimen and the supporting material, instead of reflecting completely as for a free surface, some of it will be reflected and some of it will be transmitted, depending on the impedances of the two materials. The supporting plate has a higher impedance than the target, which implies that the reflected wave will be compressive and will thus increase the stress inside the target. This is the smart thing about this approach, as it enables us to generate higher stresses by multiple reflections without increasing the impact velocity of the projectile plate.

What we need to figure out then is the shock velocity and particle velocity in the target after reflection.

The impedance of both materials are known (for the specimen, these were measured in the inverse flyer plate test), so we are able to predict the amount of reflection and transmission.

Further, since the impedance of the supporting plate is higher than for the specimen, the stress wave will be reflected as a compressive wave, thus increasing the stress inside the specimen. The same happens when the wave reaches the projectile, so after a few reflections we are able to reach very high stresses inside the specimen. As we see, the whole process is very similar to the SHB except for the geometry and time duration which makes sure that the stress state is one of uniaxial strain instead of uniaxial stress.

We can use the VISAR to measure the particle velocity, but again we are not measuring directly at the specimen. From the first pulse, we find the particle velocity in the specimen after interaction with the supporting plate. However, since we know the impedance for both materials, we can use this to calculate the stress state in the specimen right after impact. Further, knowing the impedance for each reflection/transmission we can interpret the measured back face velocity to find both the various shock velocities and particles velocities (for each reflection). Thus, we can obtain the EOS for very high pressures.

9 SUMMARY

We have now examined the theory behind the most important material tests. It is seen that by having access to all the various testing equipment, it will be possible to deduct quite a bit of information about a particular material. In Figure 9.1 is a summary of the information which can be obtained from the various tests. There are of course much more that could be said on the subject of material testing, but this is beyond the scope of the present report. For more details, the reader is referred to the references.

Much of the material testing equipment is very expensive and for most research institutes it is not practical to invest in all kinds of equipment. For example, the only equipment for concrete testing at FFI is a GREAC cell for static triaxial tests. During Project 766 it was decided that it would be more cost–efficient to co–operate with other institutions for dynamic tests, rather than make huge investments in Split Hopkinson Bar and Flyer Plate set–ups.

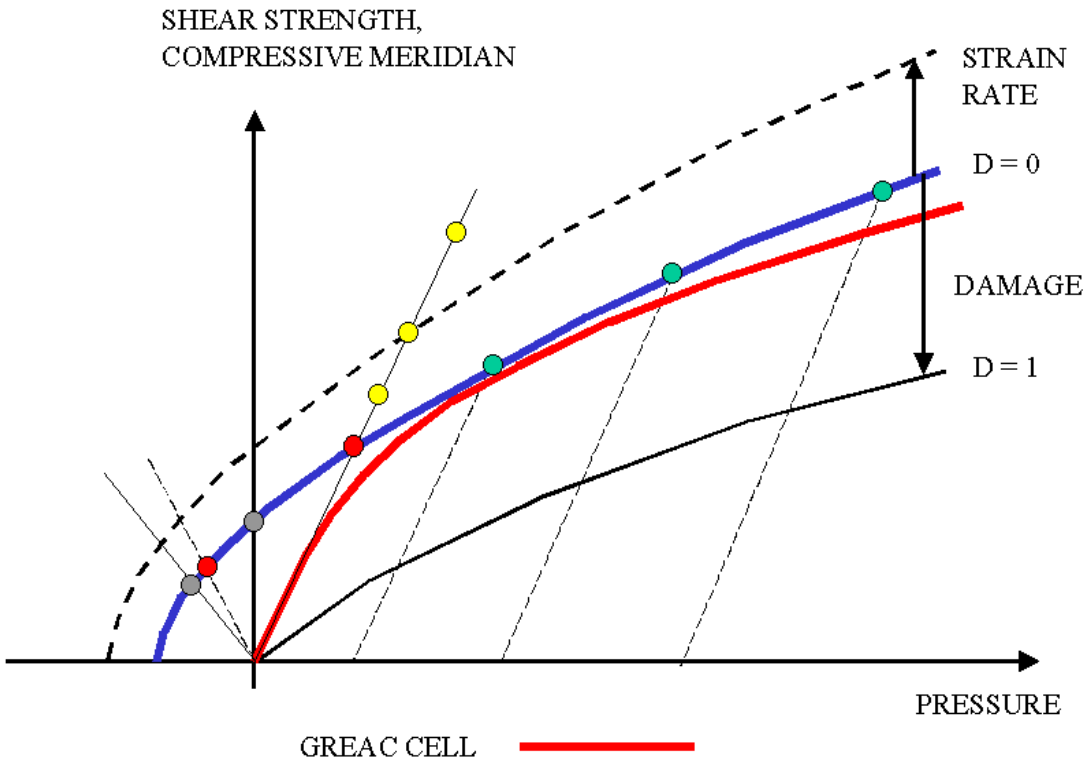

Figure 9.1: Summary of material data which can be derived from various static and dynamic material tests.

Red datapoints:	*Standard uniaxial compression and tensile tests*
Red curve:	*GREAC cell measurements*
Yellow datapoints:	*Strain rate dependent uniaxial stress tests (SHB)*
Green datapoints:	*Triaxial compression test (HOEK–cell)*
Blue curve:	*Actual yield curve of the material*

References

(1) Teland J A, A Review of Analytical Penetration Mechanics, FFI/RAPPORT–99/01264

(2) Rusås P O, Teland J A, Matlab Toolbox for Processing of GREAC cell data, FFI/RAPPORT–2000/02032

(3) Frew D J, Forrestal M J, Chen W, A Split Hopkinson Pressure Bar Technique to Determine Compressive Stress–strain Data for Rock Materials, Experimental Mechanics, Vol. 41, No. 1, March 2001

(4) Riedel W, Beton unter dynamischen Lasten – Meso– und makromechanische Modelle und ihre Parameter, EMI–Bericht 6/00

(5) Neville A M, Properties of concrete, Longman Group, Harlow Essex, 1995

(6) Svinsås E, Teland J A, Euclid RTP 14.08 / Thales JP 14.15; Firing tests of anti bunker artillery shell – Summary of material tests for concrete, FFI/RAPPORT–2002/04155

(7) Lok T S, Zhao P, Li X, Liu D, Lim C H, Effect of shaped impactor on the loading waveform in a large diameter Split Hopkinson Pressure Bar, Proceedings of the 10th Int Symposium of the Effects of Interaction of Munitions with Structures, San Diego USA, 2001

(8) Meyers M A, Dynamic Behvavior of Materials, Wiley–Interscience, 1994

(9) Gary G, Bailly G, Gatuingt F, Testing concrete at high strains and high rates of strain, Proceedings of the 3rd Int Symposium on Impact Engineering, Singapore, December 1998

(10) Bhushan B, Jahsman W E, Int J Solids Struct, 14, 739, 1978

(11) Bacon C, Separation of waves propagating in an elastic or viscoelastic Hopkinson pressure bar with three–dimensional effects, Int J Impact Engng 22, pp. 55–69, 1999

(12) Teland J A, A Review of Analytical Penetration Mechanics, FFI/RAPPORT–99/01264

(13) Rusås P O, Teland J A, Matlab Toolbox for Processing of GREAC cell data, FFI/RAPPORT–2000/02032

(14) Frew D J, Forrestal M J, Chen W, A Split Hopkinson Pressure Bar Technique to Determine Compressive Stress–strain Data for Rock Materials, Experimental Mechanics, Vol. 41, No. 1, March 2001

(15) Riedel W, Beton unter dynamischen Lasten – Meso– und makromechanische Modelle und ihre Parameter, EMI–Bericht 6/00

(16) Neville A M, Properties of concrete, Longman Group, Harlow Essex, 1995

(17) Svinsås E, Teland J A, Euclid RTP 14.08 / Thales JP 14.15; Firing tests of anti bunker artillery shell – Summary of material tests for concrete, FFI/RAPPORT–2002/04155

(18) Lok T S, Zhao P, Li X, Liu D, Lim C H, Effect of shaped impactor on the loading waveform in a large diameter Split Hopkinson Pressure Bar, Proceedings of the 10th Int Symposium of the Effects of Interaction of Munitions with Structures, San Diego USA, 2001

(19) Meyers M A, Dynamic Behvavior of Materials, Wiley–Interscience, 1994

(20) Gary G, Bailly G, Gatuingt F, Testing concrete at high strains and high rates of strain, Proceedings of the 3rd Int Symposium on Impact Engineering, Singapore, December 1998

(21) Bhushan B, Jahsman W E, Int J Solids Struct, 14, 739, 1978

(22) Bacon C, Separation of waves propagating in an elastic or viscoelastic Hopkinson pressure bar with three–dimensional effects, Int J Impact Engng 22, pp. 55–69, 1999